NASA Technical Memorandum 107190

Further Development of a New, Flux-Conserving Newton Scheme for the Navier-Stokes Equations

James R. Scott
Lewis Research Center
Cleveland, Ohio

March 1996

National Aeronautics and
Space Administration

Further Development of a New, Flux-Conserving Newton Scheme for the Navier-Stokes Equations

James R. Scott
NASA Lewis Research Center
21000 Brookpark Road, Cleveland, Ohio 44135

Abstract

This paper is one of a series of papers describing the development of a new numerical approach for solving the steady Navier-Stokes equations. The key features in the current development are (i) the discrete representation of the dependent variables by way of high order polynomial expansions, (ii) the retention of all derivatives in the expansions as unknowns to be explicitly solved for, (iii) the automatic balancing of fluxes at cell interfaces, and (iv) the discrete simulation of both the integral and differential forms of the governing equations. The main purpose of this paper is, first, to provide a systematic and rigorous derivation of the conditions that are used to simulate the differential form of the Navier-Stokes equations, and second, to extend our previously-presented internal flow scheme to external flows and nonuniform grids. Numerical results are presented for high-Reynolds-number flow (Re = 100,000) around a finite flat plate, and detailed comparisons are made with the Blasius flat plate solution and Goldstein wake solution. It is shown that the error in the streamwise velocity decreases like $r^{\alpha}\,\Delta y^2$, where $\alpha \approx 0.25$ and $r = \frac{\Delta y}{\Delta x}$ is the grid aspect ratio.

I. Introduction

This paper is concerned with the continued development of a new numerical approach for solving the steady Navier-Stokes equations and other conservation laws of the form

$$\frac{\partial \vec{h}^x}{\partial x} + \frac{\partial \vec{h}^y}{\partial y} = 0. \tag{1.1}$$

The key features in the current development are (i) the representation of the discrete unknowns by way of high order polynomial expansions; (ii) the retention of all derivatives in the polynomial expansions as unknowns to be explicitly solved for; (iii) the automatic balancing of fluxes at cell interfaces without the use of flux limiters or reconstruction; and (iv) the discrete simulation of both the integral and differential forms of the governing conservation laws.

In a previous paper (Scott et al, 1995), we formulated a quadratic-expansion discretization for the two-dimensional, compressible Navier-Stokes equations. A specific scheme was constructed for laminar channel flow, and it was shown that the developing boundary

layer could be accurately resolved on relatively coarse grids (as few as six cells per channel width).

The main purpose of this paper is, first, to provide a systematic and rigorous derivation of the conditions that are used to simulate the differential form of the Navier-Stokes equations, and second, to extend our previously-presented internal flow scheme to external flows and nonuniform grids. Specifically, we (i) derive error bounds for the *order-N* Taylor series expansion of the exact solution to equation (1.1); (ii) formalize what is meant by a discrete polynomial solution to a conservation law and introduce a generalized concept of convergence; (iii) derive necessary conditions for a discrete polynomial solution of (1.1) to converge to the corresponding exact solution; and (iv) construct a scheme for high-Reynolds-number flow past a flat plate airfoil, and show through comparison with the Blasius solution that the streamwise velocity is obtained to order $r^{\alpha}\,\Delta y^2$, where $\alpha \approx 0.25$ and $r = \frac{\Delta y}{\Delta x}$ is the grid aspect ratio.

Sections II A. and B. below serve primarily as a review of our original formulation (Scott et al, 1995). However, here we limit ourselves to incompressible flow, and introduce a generalized flux vector notation which simplifies some of the derivations. In Section II C., we deal with items (i) - (iii) as outlined in the preceding paragraph, and Section III deals with item (iv).

II. Discretization of the Navier-Stokes Equations

A. Incompressible Navier-Stokes Equations

We consider the two-dimensional, steady, incompressible Navier-Stokes equations in dimensionless form. We assume that the viscosity μ is constant, and denote the density by ρ and the Reynolds number by Re_L, where $Re_L = \frac{\rho U_\infty L}{\mu}$. The parameters L and U_∞ refer to some reference length and velocity, respectively.

Let x and y denote the horizontal and vertical coordinates, respectively, of a two-dimensional Euclidean space E_2. Denoting the horizontal velocity component by u, the vertical velocity component by v, and the static pressure by p, the governing equations for the conservation of mass and momentum may be written in Cartesian coordinates as (Anderson et al 1984)

$$\frac{\partial u}{\partial x} + \frac{\partial v}{\partial y} = 0 \tag{2.1}$$

$$\frac{\partial}{\partial x}(u^2 + p - \tau_{xx}) + \frac{\partial}{\partial y}(u\,v - \tau_{xy}) = 0 \tag{2.2}$$

$$\frac{\partial}{\partial x}(u\,v - \tau_{xy}) + \frac{\partial}{\partial y}(v^2 + p - \tau_{yy}) = 0 \tag{2.3}$$

where

$$\tau_{xx} = \frac{2}{3Re_L}(2\frac{\partial u}{\partial x} - \frac{\partial v}{\partial y}) \tag{2.4}$$

$$\tau_{xy} = \frac{1}{Re_L}(\frac{\partial u}{\partial y} + \frac{\partial v}{\partial x}) \tag{2.5}$$

$$\tau_{yy} = \frac{2}{3Re_L}(2\frac{\partial v}{\partial y} - \frac{\partial u}{\partial x}) \tag{2.6}$$

(Although $\frac{\partial v}{\partial y}$ or $\frac{\partial u}{\partial x}$ may be eliminated from τ_{xx} and τ_{yy} using (2.1), we retain both terms here to be consistent with our original compressible formulation.)

The integral form of equations (2.1) – (2.3) is given by

$$\oint_{S(V)} \vec{h}_M \cdot \overrightarrow{ds} = 0 \tag{2.7}$$

$$\oint_{S(V)} \vec{h}_{XM} \cdot \overrightarrow{ds} = 0 \tag{2.8}$$

$$\oint_{S(V)} \vec{h}_{YM} \cdot \overrightarrow{ds} = 0 \tag{2.9}$$

where the flux vectors, $\vec{h}_M$, $\vec{h}_{XM}$, and $\vec{h}_{YM}$, corresponding to the conservation of mass, x-momentum, and y-momentum, respectively, are defined by

$$\vec{h}_M \stackrel{def}{=} (u, v) \tag{2.10}$$

$$\vec{h}_{XM} \stackrel{def}{=} (u^2 + p - \tau_{xx}, uv - \tau_{xy}) \tag{2.11}$$

$$\vec{h}_{YM} \stackrel{def}{=} (uv - \tau_{xy}, v^2 + p - \tau_{yy}). \tag{2.12}$$

$S(V)$ is the boundary of an arbitrary region V in E_2, and $\overrightarrow{ds}$ is equal to $d\sigma\, \vec{n}$, where $\vec{n}$ is the outward unit normal to $S(V)$ and $d\sigma$ is the length of a surface element of $S(V)$. Equations (2.1) – (2.3) and (2.7) – (2.9) are the differential and integral conservation laws, respectively, for the conservation of mass and momentum in two space dimensions.

B. Discrete Flux Conservation Equations – Integral Formulation

Let E_2 be discretized by a mesh with nonoverlapping rectangular regions. We assume for the time being that the mesh spacing is uniform in each coordinate direction. (See Figure 1.) Each of the rectangular regions in the mesh is referred to as both a conservation element and a solution element (Chang, 1995). A conservation element is a discrete region in E_2 over which the discrete analogue of the integral conservation laws (2.7) - (2.9) is imposed. A solution element is a discrete region in E_2 in which a local polynomial expansion is employed to represent the physical solution. In general, they need not refer to the same discrete region. A conservation element is denoted by $CE(i,j)$ and a solution element by $SE(i,j)$. The boundary of a conservation element is denoted by $S(CE(i,j))$, and its cell center by (x_i, y_j).

We assume that the velocity and pressure can be represented on each $SE(i,j)$ by a polynomial expansion of degree two about the cell center (x_i, y_j), as follows:

$$\underset{\sim}{u}(x,y;i,j) \stackrel{def}{=} u_{0,0} + u_{1,0}(x-x_i) + u_{0,1}(y-y_j) + u_{2,0}(x-x_i)^2 + u_{1,1}(x-x_i)(y-y_j) + u_{0,2}(y-y_j)^2 \tag{2.13}$$

$$\underset{\sim}{v}(x,y;i,j) \stackrel{def}{=} v_{0,0} + v_{1,0}(x-x_i) + v_{0,1}(y-y_j) + v_{2,0}(x-x_i)^2 + v_{1,1}(x-x_i)(y-y_j) + v_{0,2}(y-y_j)^2 \tag{2.14}$$

$$\underset{\sim}{p}(x,y;i,j) \stackrel{def}{=} p_{0,0} + p_{1,0}(x-x_i) + p_{0,1}(y-y_j) + p_{2,0}(x-x_i)^2 + p_{1,1}(x-x_i)(y-y_j) + p_{0,2}(y-y_j)^2. \tag{2.15}$$

For clarity, the i,j subscripts have been omitted from the coefficients in the local polynomial expansions. These coefficients are the unknowns to be solved for. They are related to the discrete derivatives (at the cell center) by

$$u_{0,0} = \underset{\sim}{u} \tag{2.16}$$

$$u_{1,0} = \partial \underset{\sim}{u}/\partial x \tag{2.17}$$

$$u_{0,1} = \partial \underset{\sim}{u}/\partial y \tag{2.18}$$

$$u_{2,0} = \frac{1}{2}\,\partial^2 \underset{\sim}{u}/\partial x^2 \tag{2.19}$$

$$u_{1,1} = \partial^2 \underset{\sim}{u}/\partial x \partial y \tag{2.20}$$

$$u_{0,2} = \frac{1}{2}\,\partial^2 \underset{\sim}{u}/\partial y^2, \tag{2.21}$$

and similarly for $\underset{\sim}{v}$ and $\underset{\sim}{p}$.

The discrete analogue to equations (2.7) - (2.9) in E_2 is then given by

$$\oint_{S(CE(i,j))} \vec{\underset{\sim}{h}}_M \cdot \vec{ds} = 0 \tag{2.22}$$

$$\oint_{S(CE(i,j))} \vec{\underset{\sim}{h}}_{XM} \cdot \vec{ds} = 0 \tag{2.23}$$

$$\oint_{S(CE(i,j))} \vec{\underset{\sim}{h}}_{YM} \cdot \vec{ds} = 0 \tag{2.24}$$

where

$$\vec{\underset{\sim}{h}}_M \stackrel{def}{=} (\underset{\sim}{u}, \underset{\sim}{v}) \tag{2.25}$$

$$\vec{\underset{\sim}{h}}_{XM} \stackrel{def}{=} (\underset{\sim}{u}^2 + \underset{\sim}{p} - \underset{\sim}{\tau}_{xx}, \underset{\sim}{u}\,\underset{\sim}{v} - \underset{\sim}{\tau}_{xy}) \tag{2.26}$$

$$\vec{\underset{\sim}{h}}_{YM} \stackrel{def}{=} (\underset{\sim}{u}\,\underset{\sim}{v} - \underset{\sim}{\tau}_{xy}, \underset{\sim}{v}^2 + \underset{\sim}{p} - \underset{\sim}{\tau}_{yy}) \tag{2.27}$$

and

$$\underset{\sim}{\tau}_{xx} = \frac{2}{3Re_L}(2\,\partial\underset{\sim}{u}/\partial x - \partial\underset{\sim}{v}/\partial y) \tag{2.28}$$

$$\underset{\sim}{\tau}_{xy} = \frac{1}{Re_L}(\partial\underset{\sim}{u}/\partial y + \partial\underset{\sim}{v}/\partial x) \tag{2.29}$$

$$\underset{\sim}{\tau}_{yy} = \frac{2}{3Re_L}(2\,\partial\underset{\sim}{v}/\partial y - \partial\underset{\sim}{u}/\partial x). \tag{2.30}$$

Equations (2.22) – (2.24) are a coupled system of integral conservation laws in which the fluxes $\vec{\underset{\sim}{h}}_M \cdot \overrightarrow{ds}$, $\vec{\underset{\sim}{h}}_{XM} \cdot \overrightarrow{ds}$, and $\vec{\underset{\sim}{h}}_{YM} \cdot \overrightarrow{ds}$ are conserved by way of the discrete variables $\underset{\sim}{u}, \underset{\sim}{v}$ and $\underset{\sim}{p}$. Each equation takes the form

$$\oint_{S(CE(i,j))} \vec{\underset{\sim}{h}} \cdot \overrightarrow{ds} = 0, \tag{2.31}$$

where the second-order expansion $\vec{\underset{\sim}{h}}$ is a function of $\underset{\sim}{u}$, $\underset{\sim}{v}$ and $\underset{\sim}{p}$. Since the form of each integral in (2.22) – (2.24) is identical, the integrations may be carried out by way of equation (2.31), where

$$\vec{\underset{\sim}{h}} \stackrel{def}{=} (\underset{\sim}{h}^x, \underset{\sim}{h}^y) \tag{2.32}$$

and

$$\begin{aligned}\underset{\sim}{h}^x(x,y;i,j) \stackrel{def}{=}\ & h^x_{0,0} + h^x_{1,0}(x-x_i) + h^x_{0,1}(y-y_j) \\ & + h^x_{2,0}(x-x_i)^2 + h^x_{1,1}(x-x_i)(y-y_j) + h^x_{0,2}(y-y_j)^2\end{aligned} \tag{2.33}$$

$$\begin{aligned}\underset{\sim}{h}^y(x,y;i,j) \stackrel{def}{=}\ & h^y_{0,0} + h^y_{1,0}(x-x_i) + h^y_{0,1}(y-y_j) \\ & + h^y_{2,0}(x-x_i)^2 + h^y_{1,1}(x-x_i)(y-y_j) + h^y_{0,2}(y-y_j)^2.\end{aligned} \tag{2.34}$$

It is understood that each of the coefficients in (2.33) and (2.34) are functions of the discrete variables $u_{0,0}$, $v_{0,0}$, $p_{0,0}$, $u_{1,0}$, $v_{1,0}$, $p_{1,0}$, etc.. For example, when $\vec{\underset{\sim}{h}}$ corresponds to $\vec{\underset{\sim}{h}}_{XM}$, the term $h^x_{0,0}$ corresponds to the constant term of the expression $\underset{\sim}{u}^2 + \underset{\sim}{p} - \underset{\sim}{\tau}_{xx}$, and similarly for the other terms. Once the results are obtained in terms of $\vec{\underset{\sim}{h}}$, it is a simple

matter to derive the corresponding results for $\vec{\underset{\sim}{h}}_M$, $\vec{\underset{\sim}{h}}_{xM}$, and $\vec{\underset{\sim}{h}}_{yM}$ by way of equations (2.25) – (2.27).

Since the boundary $S(CE(i,j))$ of each conservation element is a simple closed curve in E_2, the surface integration required in equation (2.31) can be converted into a simple contour integral. With $\overrightarrow{ds} = d\sigma\,\vec{n}$, where $\vec{n}$ is the outward unit normal to $S(CE(i,j))$ and $d\sigma$ is the length of a surface element in E_2, we have

$$\overrightarrow{ds} \stackrel{def}{=} dy\,\vec{i} - dx\,\vec{j}, \tag{2.35}$$

and

$$\vec{\underset{\sim}{h}} \cdot \overrightarrow{ds} = -\underset{\sim}{h}^y\,dx + \underset{\sim}{h}^x\,dy = \vec{\underset{\sim}{g}} \cdot \vec{dr} \tag{2.36}$$

where

$$\vec{\underset{\sim}{g}} \stackrel{def}{=} (-\underset{\sim}{h}^y, \underset{\sim}{h}^x) \tag{2.37}$$

and

$$\vec{dr} \stackrel{def}{=} dx\,\vec{i} + dy\,\vec{j}. \tag{2.38}$$

The line integration is taken to be positive in the counterclockwise sense. If we denote the vertices of an arbitrary conservation element $CE(i,j)$ by P, Q, R, and S as shown in Figure 2, we have

$$\oint_{S(CE(i,j))} \vec{\underset{\sim}{h}} \cdot \overrightarrow{ds} = \oint_{PQRS_{i,j}} \vec{\underset{\sim}{g}} \cdot \vec{dr}$$

$$\stackrel{def}{=} \left[J(\overline{PQ}) + J(\overline{QR}) + J(\overline{RS}) + J(\overline{SP})\right]_{i,j}. \tag{2.39}$$

$[J(\overline{PQ})]_{i,j}$ denotes the flux of $\vec{\underset{\sim}{h}}$ through the line segment $\overline{PQ}_{i,j}$, and similarly for $J(\overline{QR})$, $J(\overline{RS})$, and $J(\overline{SP})$. We then have (omitting i,j subscripts)

$$J(\overline{PQ}) \stackrel{def}{=} \int_P^Q -\underset{\sim}{h}^y\,dx + \underset{\sim}{h}^x\,dy = \int_{x_i-\frac{\Delta x}{2}}^{x_i+\frac{\Delta x}{2}} \underset{\sim}{h}^y\,dx \qquad \text{with} \quad y = y_j + \frac{\Delta y}{2}. \tag{2.40}$$

Similarly,

$$J(\overline{QR}) \stackrel{def}{=} -\int_{y_j-\frac{\Delta y}{2}}^{y_j+\frac{\Delta y}{2}} \underset{\sim}{h}^x\,dy \qquad \text{with} \quad x = x_i - \frac{\Delta x}{2} \tag{2.41}$$

$$J(\overline{RS}) \stackrel{def}{=} -\int_{x_i-\frac{\Delta x}{2}}^{x_i+\frac{\Delta x}{2}} \underset{\sim}{h}^y\,dx \qquad \text{with} \quad y = y_j - \frac{\Delta y}{2} \tag{2.42}$$

$$J(\overline{SP}) \stackrel{def}{=} \int_{y_j-\frac{\Delta y}{2}}^{y_j+\frac{\Delta y}{2}} \underset{\sim}{h}^x\,dy \qquad \text{with} \quad x = x_i + \frac{\Delta x}{2}. \tag{2.43}$$

Carrying out the line integrations in equations (2.40) - (2.43), one obtains

$$J(\overline{PQ}) = \frac{\Delta x^3}{12} h^y_{2,0} + \Delta x \left[\frac{\Delta y^2}{4} h^y_{0,2} + \frac{\Delta y}{2} h^y_{0,1} + h^y_{0,0}\right] \tag{2.44}$$

$$J(\overline{QR}) = -\frac{\Delta y^3}{12} h^x_{0,2} - \Delta y \left[\frac{\Delta x^2}{4} h^x_{2,0} - \frac{\Delta x}{2} h^x_{1,0} + h^x_{0,0}\right] \tag{2.45}$$

$$J(\overline{RS}) = -\frac{\Delta x^3}{12} h^y_{2,0} - \Delta x \left[\frac{\Delta y^2}{4} h^y_{0,2} - \frac{\Delta y}{2} h^y_{0,1} + h^y_{0,0}\right] \tag{2.46}$$

$$J(\overline{SP}) = \frac{\Delta y^3}{12} h^x_{0,2} + \Delta y \left[\frac{\Delta x^2}{4} h^x_{2,0} + \frac{\Delta x}{2} h^x_{1,0} + h^x_{0,0}\right]. \tag{2.47}$$

By virtue of equations (2.31) and (2.39) we require that

$$J(\overline{PQ}) + J(\overline{QR}) + J(\overline{RS}) + J(\overline{SP}) \equiv 0. \tag{2.48}$$

Thus, we obtain the *flux conservation constraint*

$$h^x_{1,0} + h^y_{0,1} = 0. \tag{2.49}$$

Imposing this condition, we obtain the following expressions for the normalized flux of $\vec{h}$ across the boundaries of $CE(i,j)$:

$$\frac{J(\overline{PQ})}{\Delta x} = \frac{\Delta x^2}{12} h^y_{2,0} + \frac{\Delta y^2}{4} h^y_{0,2} - \frac{\Delta y}{2} h^x_{1,0} + h^y_{0,0} \tag{2.50}$$

$$-\frac{J(\overline{QR})}{\Delta y} = \frac{\Delta y^2}{12} h^x_{0,2} + \frac{\Delta x^2}{4} h^x_{2,0} - \frac{\Delta x}{2} h^x_{1,0} + h^x_{0,0} \tag{2.51}$$

$$-\frac{J(\overline{RS})}{\Delta x} = \frac{\Delta x^2}{12} h^y_{2,0} + \frac{\Delta y^2}{4} h^y_{0,2} + \frac{\Delta y}{2} h^x_{1,0} + h^y_{0,0} \tag{2.52}$$

$$\frac{J(\overline{SP})}{\Delta y} = \frac{\Delta y^2}{12} h^x_{0,2} + \frac{\Delta x^2}{4} h^x_{2,0} + \frac{\Delta x}{2} h^x_{1,0} + h^x_{0,0}. \tag{2.53}$$

The flux expressions above may now be expressed in terms of the discrete dependent variables of the Navier-Stokes equations by way of equations (2.25) – (2.27). Corresponding to (2.25), we have

$$\underset{\sim}{\vec{h}} = \underset{\sim}{\vec{h}}_M \tag{2.54}$$

so that

$$\underset{\sim}{h}^x = \underset{\sim}{u} \qquad \underset{\sim}{h}^y = \underset{\sim}{v} \tag{2.55a,b}$$

and the mass flux conservation constraint corresponding to (2.49) is

$$u_{1,0} + v_{0,1} = 0. \tag{2.56}$$

The normalized fluxes for $\vec{\underset{\sim}{h}}_M$ are given by (2.50) – (2.53), where $h^x_{0,0} = u_{0,0}$, $h^y_{0,0} = v_{0,0}$, etc.

Corresponding to (2.26), we have

$$\vec{\underset{\sim}{h}} = \vec{\underset{\sim}{h}}_{XM} \tag{2.57}$$

where

$$\underset{\sim}{h}^x = \underset{\sim}{u}^2 + \underset{\sim}{p} - \underset{\sim}{\tau}_{xx} \qquad \underset{\sim}{h}^y = \underset{\sim}{u}\,\underset{\sim}{v} - \underset{\sim}{\tau}_{xy}. \tag{2.58a,b}$$

The x-momentum flux conservation constraint corresponding to (2.49) is

$$u_{1,0}\,u_{0,0} + u_{0,1}\,v_{0,0} + p_{1,0} - \frac{1}{Re_L}[(2\,u_{0,2} + v_{1,1}) + \frac{2}{3}(4\,u_{2,0} - v_{1,1})] = 0, \tag{2.59}$$

and the flux expressions for $\vec{\underset{\sim}{h}}_{XM}$ are readily obtained by way of equations (2.58) and (2.50) – (2.53). Thus, one easily obtains the x-momentum flux through the right hand face of a conservation element,

$$\frac{J(\overline{SP})_{XM}}{\Delta y} = \tag{2.60}$$

$$\frac{\Delta y^2}{12}(2\,u_{0,2}\,u_{0,0} + u^2_{0,1} + p_{0,2}) + \frac{\Delta x^2}{4}(2\,u_{2,0}\,u_{0,0} + u^2_{1,0} + p_{2,0})$$

$$- \frac{\Delta x}{2}\Big[v_{0,0}\,u_{0,1} + u_{0,0}\,v_{0,1} - \frac{1}{Re_L}(2\,u_{0,2} + v_{1,1})\Big] + u^2_{0,0} + p_{0,0} - \frac{2}{3Re_L}(2\,u_{1,0} - v_{0,1}),$$

and similar expressions for the remaining fluxes. (Here $h^x_{1,0}$ has been replaced with $-h^y_{0,1}$ because it gives a simpler expression.)

Similarly, corresponding to (2.27),

$$\vec{\underset{\sim}{h}} = \vec{\underset{\sim}{h}}_{YM} \tag{2.61}$$

with

$$\underset{\sim}{h}^x = \underset{\sim}{u}\,\underset{\sim}{v} - \underset{\sim}{\tau}_{xy} \qquad \underset{\sim}{h}^y = \underset{\sim}{v}^2 + \underset{\sim}{p} - \underset{\sim}{\tau}_{yy}. \tag{2.62a,b}$$

The y-momentum flux conservation constraint is

$$v_{1,0}\,u_{0,0} + v_{0,1}\,v_{0,0} + p_{0,1} - \frac{1}{Re_L}[(2\,v_{2,0} + u_{1,1}) + \frac{2}{3}(4\,v_{0,2} - u_{1,1})] = 0, \tag{2.63}$$

and the flux of $\vec{\underset{\sim}{h}}_{YM}$ through the right hand face of a conservation element is given by

$$\frac{J(\overline{SP})_{YM}}{\Delta y} = \tag{2.64}$$

$$\frac{\Delta y^2}{12}(v_{0,2}\,u_{0,0} + u_{0,2}\,v_{0,0} + v_{0,1}\,u_{0,1}) + \frac{\Delta x^2}{4}(v_{2,0}\,u_{0,0} + u_{2,0}\,v_{0,0} + v_{1,0}\,u_{1,0})$$

$$+ \frac{\Delta x}{2}\Big[u_{0,0}\,v_{1,0} + v_{0,0}\,u_{1,0} - \frac{1}{Re_L}(2\,v_{2,0} + u_{1,1})\Big] + u_{0,0}\,v_{0,0} - \frac{1}{Re_L}(u_{0,1} + v_{1,0}).$$

The following conditions are then satisfied on each conservation element:

$$J(\overline{PQ})_M + J(\overline{QR})_M + J(\overline{RS})_M + J(\overline{SP})_M \equiv 0 \tag{2.65}$$

$$J(\overline{PQ})_{XM} + J(\overline{QR})_{XM} + J(\overline{RS})_{XM} + J(\overline{SP})_{XM} \equiv 0 \tag{2.66}$$

$$J(\overline{PQ})_{YM} + J(\overline{QR})_{YM} + J(\overline{RS})_{YM} + J(\overline{SP})_{YM} \equiv 0. \tag{2.67}$$

The above formulation provides the framework through which integral flux conservation is achieved. We may now turn our attention to the differential conservation laws (2.1) – (2.3).

C. Discrete Flux Conservation Equations – Differential Formulation

In the previous section, we derived the local constraint (2.49),

$$h^x_{1,0} + h^y_{0,1} = 0,$$

to ensure that the discrete flux vector $\vec{h}$ (defined by (2.32) – (2.34)) satisfies

$$\oint_{S(CE(i,j))} \vec{h} \cdot \vec{ds} = 0.$$

Now we observe that, by virtue of (2.49), $\vec{h}$ also satisfies

$$\vec{\nabla} \cdot \vec{h} = 0 \qquad \text{at } (x,y) = (x_i, y_j),$$

i.e., the differential conservation law is satisfied at the cell center.

Suppose that we further require $\vec{h}$ to satisfy $\vec{\nabla} \cdot \vec{h} = 0$ identically throughout each $SE(i,j)$. Then one obtains two additional local constraints,

$$2\,h^x_{2,0} + h^y_{1,1} = 0 \tag{2.68}$$

$$h^x_{1,1} + 2\,h^y_{0,2} = 0. \tag{2.69}$$

Our main objective in this section is to rigorously derive the above two constraints from first principles. We show, in particular, that enforcement of these constraints ensures the satisfaction of necessary conditions for the discrete second derivatives to converge to their analytical counterparts.

Throughout this section, we shall make use of the following result, which may be established by induction.

Lemma 2.1 Let $\vec{h} = (h^x, h^y)$ be defined and continuous on an open domain $\mathcal{D}$ of E_2, and let the partial derivatives of h^x and h^y exist to all orders and be continuous on $\mathcal{D}$. Then, $\vec{h}$ satisfies $\vec{\nabla} \cdot \vec{h} = 0$ throughout $\mathcal{D}$ if and only if its partial derivatives satisfy

$$\frac{\partial^n h^x}{\partial x^{n-k}\,\partial y^k}(x,y) + \frac{\partial^n h^y}{\partial x^{n-k-1}\,\partial y^{k+1}}(x,y) = 0 \tag{2.70}$$

$$\text{for } n = 1,2,3,\ldots \text{ and } k = 0,1,2,\ldots,n-1,$$

for every (x,y) in $\mathcal{D}$.

As a preliminary to what follows, we first consider the N-th order Taylor series expansion of the exact solution $\vec{h}$ of the conservation law

$$\vec{\nabla} \cdot \vec{\mathcal{H}} = 0. \tag{2.71}$$

We assume that $\vec{h} = (h^x, h^y)$ satisfies (2.71) throughout some open domain $\mathcal{D}$ of E_2, and that $\vec{h}$ is analytic throughout $\mathcal{D}$. Let $\vec{h}_N$ denote the N-th order Taylor series expansion of $\vec{h}$ about a point (x_0, y_0) in $\mathcal{D}$. Then

$$h_N^x(x,y) = \sum_{n=0}^{N}\sum_{k=0}^{n}\Big[\frac{\partial^n h^x}{\partial x^{n-k}\partial y^k}(x_0,y_0)\Big]\frac{(x-x_0)^{n-k}}{(n-k)!}\,\frac{(y-y_0)^k}{k!} \tag{2.72}$$

and

$$h_N^y(x,y) = \sum_{n=0}^{N}\sum_{k=0}^{n}\Big[\frac{\partial^n h^y}{\partial x^{n-k}\partial y^k}(x_0,y_0)\Big]\frac{(x-x_0)^{n-k}}{(n-k)!}\,\frac{(y-y_0)^k}{k!}. \tag{2.73}$$

Since

$$\frac{\partial h_N^x}{\partial x} = \sum_{n=1}^{N}\sum_{k=0}^{n-1}\Big[\frac{\partial^n h^x}{\partial x^{n-k}\partial y^k}(x_0,y_0)\Big]\frac{(x-x_0)^{n-k-1}}{(n-k-1)!}\,\frac{(y-y_0)^k}{k!} \tag{2.74}$$

and

$$\begin{aligned}\frac{\partial h_N^y}{\partial y} &= \sum_{n=1}^{N}\sum_{k=1}^{n}\Big[\frac{\partial^n h^y}{\partial x^{n-k}\partial y^k}(x_0,y_0)\Big]\frac{(x-x_0)^{n-k}}{(n-k)!}\,\frac{(y-y_0)^{(k-1)}}{(k-1)!} \\ &= \sum_{n=1}^{N}\sum_{k=0}^{n-1}\Big[\frac{\partial^n h^y}{\partial x^{n-k-1}\partial y^{k+1}}(x_0,y_0)\Big]\frac{(x-x_0)^{n-k-1}}{(n-k-1)!}\,\frac{(y-y_0)^k}{k!},\end{aligned} \tag{2.75}$$

it follows from *Lemma 2.1* that $\vec{h}_N$ is a solution of equation (2.71). We will refer to $\vec{h}_N$ as the *exact order-N solution* of (2.71).

Let (x,y) be another point in $\mathcal{D}$. Then, as an approximation to the exact solution $\vec{h}$ at (x,y), the error in $\vec{h}_N$ is given by

$$h^x(x,y) - h_N^x(x,y) = \sum_{k=0}^{N+1}\Big[\frac{\partial^{N+1}h^x}{\partial x^{N+1-k}\partial y^k}(x_1^*,y_1^*)\Big]\frac{(x-x_0)^{N+1-k}}{(N+1-k)!}\,\frac{(y-y_0)^k}{k!} \tag{2.76}$$

$$h^y(x,y) - h_N^y(x,y) = \sum_{k=0}^{N+1}\Big[\frac{\partial^{N+1}h^y}{\partial x^{N+1-k}\partial y^k}(x_2^*,y_2^*)\Big]\frac{(x-x_0)^{N+1-k}}{(N+1-k)!}\,\frac{(y-y_0)^k}{k!} \tag{2.77}$$

where (x_1^*,y_1^*) and (x_2^*,y_2^*) are points on the line segment between (x_0,y_0) and (x,y) (Buck, 1978).

Now suppose that

$$\Big|\frac{\partial^{N+1}h^x}{\partial x^{N+1-k}\partial y^k}\Big| \le M_{N+1,k} \quad \text{and} \quad \Big|\frac{\partial^{N+1}h^y}{\partial x^{N+1-k}\partial y^k}\Big| \le M_{N+1,k} \tag{2.78}$$

in a neighborhood N_0 of (x_0,y_0) for $k=0,1,...,N+1$. If $\Delta x = (x-x_0)$ and $\Delta y = (y-y_0)$ where (x,y) is any point in N_0, then

$$\|\vec{h} - \vec{h}_N\|_\infty \le \sum_{k=0}^{N+1} M_{N+1,k}\frac{|\Delta x|^{N+1-k}}{(N+1-k)!}\,\frac{|\Delta y|^k}{k!}. \tag{2.79}$$

If we let

$$M_{N+1} = \sup\{M_{N+1,k}\ k=0,1,...,N+1\}, \tag{2.80}$$

we have the more conservative error estimate

$$\|\vec{h} - \vec{h}_N\|_\infty < \frac{M_{N+1}\,(N+2)\,[\max(|\Delta x|,|\Delta y|)]^{N+1}}{[(\frac{N+1}{2})!]^2} \tag{2.81}$$

where $[(\frac{N+1}{2})!]^2 \stackrel{def}{=} (\frac{N}{2})!\,(\frac{N+2}{2})!$ if N is even.

The exact order-N solution $\vec{h}_N$ is the prototype discrete polynomial approximation to the exact solution $\vec{h}$. Its order of accuracy is given by (2.81). We may now turn our attention to *approximate order-N solutions* to (2.71). We begin by formalizing the notions of "a discrete polynomial approximation" and "convergence."

Definition 2.1 Let (x_0,y_0) be a point in E_2, and let Δx and Δy be positive numbers. Let $N_{0\Delta x\Delta y} = \Big\{(x,y) : |x-x_0| \le \frac{\Delta x}{2} \text{ and } |y-y_0| \le \frac{\Delta y}{2}\Big\}$. Then, a local discrete polynomial approximation to the exact solution of equation (2.71) is a function $\underset{\sim}{\vec{h}}_N \stackrel{def}{=} (\underset{\sim}{h}{}^x_N, \underset{\sim}{h}{}^y_N)$ defined on $N_{0\Delta x\Delta y}$ by

$$\underset{\sim}{h}{}^x_N(x,y) = \sum_{n=0}^{N}\sum_{k=0}^{n} h^x_{n-k,k}(\Delta x,\Delta y)\,(x-x_0)^{n-k}\,(y-y_0)^k \tag{2.82}$$

$$\underset{\sim}{h}^y_N(x,y) \;=\; \sum_{n=0}^{N}\sum_{k=0}^{n} h^y_{n-k,k}(\Delta x,\Delta y)\,(x-x_0)^{n-k}\,(y-y_0)^k, \tag{2.83}$$

where $h^x_{n-k,k}$ and $h^y_{n-k,k}$ are functions of Δx and Δy.

Definition 2.2 A local discrete polynomial approximation $\vec{\underset{\sim}{h}}_N$ converges to order K to the exact solution $\vec{h}$ of the conservation law $\vec{\nabla}\cdot\vec{\mathcal{H}} = 0$ as $\Delta x \to 0$, $\Delta y \to 0$ if and only if for any $\epsilon > 0$, there exist numbers $\delta_1 > 0$ and $\delta_2 > 0$ such that when $\Delta x < \delta_1$ and $\Delta y < \delta_2$,

$$\left| h^x_{n-k,k}(\Delta x,\Delta y) \;-\; \frac{\partial^n h^x}{\partial x^{n-k}\partial y^k}(x_0,y_0)\,\frac{1}{(n-k)!}\,\frac{1}{k!}\right| \;<\; \epsilon \tag{2.84}$$

$$\left| h^y_{n-k,k}(\Delta x,\Delta y) \;-\; \frac{\partial^n h^y}{\partial x^{n-k}\partial y^k}(x_0,y_0)\,\frac{1}{(n-k)!}\,\frac{1}{k!}\right| \;<\; \epsilon \tag{2.85}$$

for $n = 0,1,...,K$, and $k = 0,1,...,n$, and the remainder $\vec{\underset{\sim}{R}}_K = \vec{\underset{\sim}{h}}_N - \vec{\underset{\sim}{h}}_K \to \vec{0}$ as $\Delta x \to 0$, $\Delta y \to 0$.

We may now state and prove the two following important theorems.

Theorem 2.1 Let ϵ be any positive number, and let $0 \le K \le N$. If $\vec{\underset{\sim}{h}}_N(\Delta x,\Delta y)$ converges to order K to the exact solution $\vec{h}$ of the conservation law $\vec{\nabla}\cdot\vec{\mathcal{H}} = 0$ as $\Delta x \to 0$, $\Delta y \to 0$, then for all sufficiently small Δx and Δy,

$$\|\vec{h} \;-\; \vec{\underset{\sim}{h}}_N(\Delta x,\Delta y)\|_\infty \;<\; \epsilon.$$

Proof: We have

$$\vec{h} - \vec{\underset{\sim}{h}}_N \;=\; \vec{h} \;-\vec{h}_N \;+\; \vec{h}_N \;-\; \vec{\underset{\sim}{h}}_N \tag{2.2a}$$

$$\Rightarrow \quad \|\vec{h} - \vec{\underset{\sim}{h}}_N\|_\infty \;\le\; \|\vec{h} \;-\vec{h}_N\|_\infty \;+\; \|\vec{h}_N \;-\; \vec{\underset{\sim}{h}}_N\|_\infty \tag{2.2b}$$

$$\Rightarrow \quad \|\vec{h} - \vec{\underset{\sim}{h}}_N\|_\infty \;\le\; \|\vec{h} \;-\vec{h}_N\|_\infty \;+\; \|\vec{h}_K \;-\; \vec{\underset{\sim}{h}}_K\|_\infty \;+\; \|\vec{R}_K \;-\; \vec{\underset{\sim}{R}}_K\|_\infty \tag{2.2c}$$

where $\vec{R}_K = \vec{h}_N - \vec{h}_K$ and $\vec{\underset{\sim}{R}}_K = \vec{\underset{\sim}{h}}_N - \vec{\underset{\sim}{h}}_K$. The first two terms on the right hand side of *(2.2c)* are each less than $\frac{\epsilon}{3}$ for sufficiently small Δx and Δy, and the third term is a polynomial whose lowest order term is of degree $K+1$. Since the coefficients of $\vec{R}_K$ are fixed, and $\vec{\underset{\sim}{R}}_K \to \vec{0}$, the third term is also less than $\frac{\epsilon}{3}$ for sufficiently small Δx and Δy, and the theorem follows.

Theorem 2.2 Let ϵ be any positive number, and let $1 \le K \le N$. If $\vec{\underset{\sim}{h}}_N(\Delta x,\Delta y)$ converges to order K to the exact solution $\vec{h}$ of the conservation law $\vec{\nabla}\cdot\vec{\mathcal{H}} = 0$ as $\Delta x \to 0$, $\Delta y \to 0$, then for all sufficiently small Δx and Δy,

$$(n-k)\,h^x_{n-k,k}(\Delta x,\Delta y) \;+\; (k+1)\,h^y_{n-k-1,k+1}(\Delta x,\Delta y) \;<\; \epsilon$$

for $n = 1,2,...K$, $k = 0,1,...n-1$.

Proof:

Since $\vec{\underset{\sim}{h}}_N(\Delta x, \Delta y)$ converges to order K, for any $n = 1, 2, ..., K$, and $k = 0, 1, ..., n-1$, we have

$$h^x_{n-k,k}(\Delta x, \Delta y) \;\rightarrow\; \Big[\frac{\partial^n h^x}{\partial x^{n-k}\partial y^k}(x_0, y_0)\Big] \frac{1}{(n-k)!}\,\frac{1}{k!} \tag{2.9a}$$

$$h^y_{n-k-1,k+1}(\Delta x, \Delta y) \;\rightarrow\; \Big[\frac{\partial^n h^y}{\partial x^{n-k-1}\partial y^{k+1}}(x_0, y_0)\Big] \frac{1}{(n-k-1)!}\,\frac{1}{(k+1)!} \tag{2.9b}$$

so that

$$(n-k)\, h^x_{n-k,k}(\Delta x, \Delta y) \;\rightarrow\; \Big[\frac{\partial^n h^x}{\partial x^{n-k}\partial y^k}(x_0, y_0)\Big] \frac{1}{(n-k-1)!}\,\frac{1}{k!} \tag{2.9c}$$

$$(k+1)\, h^y_{n-k-1,k+1}(\Delta x, \Delta y) \;\rightarrow\; \Big[\frac{\partial^n h^y}{\partial x^{n-k-1}\partial y^{k+1}}(x_0, y_0)\Big] \frac{1}{(n-k-1)!}\,\frac{1}{k!} \tag{2.9d}$$

$$\Rightarrow \quad (n-k)\, h^x_{n-k,k}(\Delta x, \Delta y) \;+\; (k+1)\, h^y_{n-k-1,k+1}(\Delta x, \Delta y) \tag{2.9e}$$

$$\rightarrow \Big[\frac{\partial^n h^x}{\partial x^{n-k}\partial y^k}(x_0, y_0) \;+\; \frac{\partial^n h^y}{\partial x^{n-k-1}\partial y^{k+1}}(x_0, y_0)\Big] \frac{1}{(n-k-1)!}\,\frac{1}{k!}.$$

But since $\vec{h}$ is a solution of the conservation law,

$$\Big[\frac{\partial^n h^x}{\partial x^{n-k}\partial y^k}(x_0, y_0) \;+\; \frac{\partial^n h^y}{\partial x^{n-k-1}\partial y^{k+1}}(x_0, y_0)\Big] \;=\; 0 \tag{2.9f}$$

by *Lemma 2.1.* Thus,

$$(n-k)\, h^x_{n-k,k}(\Delta x, \Delta y) \;+\; (k+1)\, h^y_{n-k-1,k+1}(\Delta x, \Delta y) \;\rightarrow\; 0 \tag{2.9g}$$

as $\Delta x \rightarrow 0$, $\Delta y \rightarrow 0$, and the theorem follows.

The meaning of *Theorem 2.2* becomes clear when we consider the divergence of $\vec{\underset{\sim}{h}}_N$. With $\vec{\underset{\sim}{h}}_N \overset{def}{=} (\underset{\sim}{h}^x_N, \underset{\sim}{h}^y_N)$ defined by (2.82) and (2.83), we have

$$\frac{\partial}{\partial x}\,\underset{\sim}{h}^x_N(x, y) \;=\; \sum_{n=1}^{N}\sum_{k=0}^{n-1} (n-k)\, h^x_{n-k,k}(x-x_0)^{n-k-1}(y-y_0)^k \tag{2.86}$$

$$\frac{\partial}{\partial y}\,\underset{\sim}{h}^y_N(x, y) \;=\; \sum_{n=1}^{N}\sum_{k=1}^{n} k\, h^y_{n-k,k}(x-x_0)^{n-k}(y-y_0)^{k-1}$$

$$=\; \sum_{n=1}^{N}\sum_{k=0}^{n-1} (k+1)\, h^y_{n-k-1,k+1}(x-x_0)^{n-k-1}(y-y_0)^k \tag{2.87}$$

so that

$$\vec{\nabla}\cdot\vec{\underset{\sim}{h}}_N \;=\; \frac{\partial}{\partial x}\,\underset{\sim}{h}^x_N(x, y) \;+\; \frac{\partial}{\partial y}\,\underset{\sim}{h}^y_N(x, y) \tag{2.88}$$

$$= \sum_{n=1}^{N} \sum_{k=0}^{n-1} \left[(n-k)\, h^x_{n-k,k} \;+\; (k+1)\, h^y_{n-k-1,k+1} \right] (x - x_0)^{n-k-1} (y - y_0)^k .$$

According to *Theorem 2.2*, a necessary condition for $\vec{\tilde{h}}_N$ to converge to order N is that

$$(n-k)\, h^x_{n-k,k} \;+\; (k+1)\, h^y_{n-k-1,k+1} \;\rightarrow\; 0 \tag{2.89}$$

as $\Delta x, \Delta y \rightarrow 0$, for $n = 1, 2, ..., N,\ k = 0, 1, ..., n-1$.

The implications of this are especially significant when it comes to numerical calculations. In general, the mechanism whereby conditions (2.89) are satisfied depends on the particular numerical method being used. Finite-difference methods, for example, satisfy each of the conditions (2.89) to a certain order through the difference approximations that are used. In this case, condition (2.89) is satisfied to a given order, say order L, for $n = 1$. Then for higher values of n, conditions (2.89) are satisfied to an order which is less than or equal to L. The higher order constraints expressed by (2.89) do not result in independent conditions for a finite-difference scheme. Rather, the higher order constraints are automatically satisfied by virtue of the difference equations employed to satisfy (2.89) corresponding to $n = 1$.

On the other hand, when one solves for the unknown coefficients $h^x_{n-k,k}$ and $h^y_{n-k,k}$ directly, as in the present approach, each constraint associated with (2.89) represents an independent condition. Thus, to ensure that (2.89) is always satisfied, one should require $h^x_{n-k,k}$ and $h^y_{n-k,k}$ to satisfy

$$(n-k)\, h^x_{n-k,k} \;+\; (k+1)\, h^y_{n-k-1,k+1} \;=\; 0 \tag{2.90}$$

for $n = 1, 2, ..., N,\ k = 0, 1, ..., n-1$. That is, $\vec{\tilde{h}}_N$ should be a solution of the conservation law, and for the special case of $N = 2$, constraints (2.68) and (2.69) should always be imposed. As a result, conditions (2.89) are not satisfied just to a certain order as in finite-difference methods, but rather are satisfied identically.

Since the coefficients $h^x_{n-k,k}$ and $h^y_{n-k,k}$ are functions of intermediate variables, each constraint associated with (2.90) must be expressed in terms of the intermediate variables. For the Navier-Stokes equations, this can be accomplished using (2.25) – (2.27). Equations (2.68) – (2.69), corresponding to the conservation of mass, x-momentum, and y-momentum, then become

$$2\, u_{2,0} \;+\; v_{1,1} \;=\; 0 \tag{2.91}$$

$$u_{1,1} \;+\; 2\, v_{0,2} \;=\; 0 \tag{2.92}$$

$$2\,(2\, u_{0,0}\, u_{2,0} \;+\; u^2_{1,0} \;+\; p_{2,0}) \;+\; u_{1,1}\, v_{0,0} \;+\; v_{1,1}\, u_{0,0} \;+\; u_{1,0}\, v_{0,1} \;+\; u_{0,1}\, v_{1,0} \;=\; 0 \tag{2.93}$$

$$2\, u_{1,1}\, u_{0,0} \;+\; 2\, u_{1,0}\, u_{0,1} \;+\; p_{1,1} \;+\; 2\,(u_{0,0}\, v_{0,2} \;+\; v_{0,0}\, u_{0,2} \;+\; v_{0,1}\, u_{0,1}) \;=\; 0 \tag{2.94}$$

$$2\,(u_{0,0}\, v_{2,0} \;+\; v_{0,0}\, u_{2,0} \;+\; v_{1,0}\, u_{1,0}) \;+\; 2\, v_{1,1}\, v_{0,0} \;+\; 2\, v_{1,0}\, v_{0,1} \;+\; p_{1,1} \;=\; 0 \tag{2.95}$$

$$u_{1,1}\,v_{0,0} + v_{1,1}\,u_{0,0} + u_{1,0}\,v_{0,1} + u_{0,1}\,v_{1,0} + 2(2\,v_{0,0}\,v_{0,2} + v_{0,1}^2 + p_{0,2}) = 0, \quad (2.96)$$

respectively. Note that these constraints ensure the satisfaction of necessary, but not sufficient, conditions for the discrete second derivatives to converge to their analytical counterparts.

III. High-Reynolds-Number Flow Past a Finite Flat Plate

We now apply the discretization outlined above to the thin airfoil boundary layer problem. Consider the mesh shown in Figure 3. The airfoil lies on the x-axis between $x = 0$ and $x = 1$, and has uniform spacing in each direction. Note that the mesh includes an upstream and wake region.

Let N_i and N_j denote the number of solution elements in the x and y directions, respectively. Then, representing u, v, and p by way of the local expansions (2.13) – (2.15), there are 18 discrete unknowns per cell, for a total of $18N_iN_j$ unknowns altogether. We thus require $18N_iN_j$ conditions to have a closed system of equations.

The flux conservation constraints (2.56), (2.59), and (2.63), together with the differential constraints (2.91) – (2.96), immediately provide $9N_iN_j$ conditions. These constraints ensure that the discrete flux vectors defined by (2.25) – (2.27) satisfy both the integral and differential forms of the governing conservation laws.

To ensure that mass and momentum are conserved globally, we must require that fluxes be conserved across cell interfaces. Using (2.51) and (2.53), the generalized statement of flux conservation across vertical interfaces is given by

$$\left[\frac{\Delta y^2}{12}\,h^x_{0,2} + \frac{\Delta x^2}{4}\,h^x_{2,0} + \frac{\Delta x}{2}\,h^x_{1,0} + h^x_{0,0}\right]_{i-1}$$

$$- \left[\frac{\Delta y^2}{12}\,h^x_{0,2} + \frac{\Delta x^2}{4}\,h^x_{2,0} - \frac{\Delta x}{2}\,h^x_{1,0} + h^x_{0,0}\right]_{i} = 0. \quad (3.1)$$

For conservation of mass, (3.1) becomes (using (2.55))

$$\left[\frac{\Delta y^2}{12}\,u_{0,2} + \frac{\Delta x^2}{4}\,u_{2,0} + \frac{\Delta x}{2}\,u_{1,0} + u_{0,0}\right]_{i-1}$$

$$- \left[\frac{\Delta y^2}{12}\,u_{0,2} + \frac{\Delta x^2}{4}\,u_{2,0} - \frac{\Delta x}{2}\,u_{1,0} + u_{0,0}\right]_{i} = 0. \quad (3.2)$$

A similar statement is obtained for mass conservation across horizontal interfaces. Using (2.58) and (2.62), one derives the analogous expressions for conservation of x and y momentum. Thus, one obtains a total of $3N_j(N_i - 1) + 3N_i(N_j - 1) - 3N_a$ interface flux conditions, where N_a is the number of solution elements between the airfoil leading and trailing edges.

Boundary conditions account for an additional $4N_i + 3N_j + 4N_a$ conditions. For each cell adjacent to the airfoil, we require the mass flux through the wall face, and the u velocity

component at the midpoint of the wall face, to be zero. At the upstream boundary we specify the velocity, and at the downstream boundary we specify the pressure. Along the free-stream boundary cells, we specify zero y gradient conditions for $\underset{\sim}{u}$ and $\underset{\sim}{v}$.

Finally, as a means of imposing the zero (constant) pressure gradient condition, we set

$$p_{1,1} = 0 \qquad p_{2,0} = 0. \tag{3.3a,b}$$

These conditions are both justified when the Reynolds number is large, since the pressure is nearly constant except near the singular leading and trailing edge regions. A scheme which retains $p_{1,1}$ and $p_{2,0}$ has also been developed and implemented (Scott et al, 1995). Numerical results for the flat plate problem have shown that $p_{1,1}$ and $p_{2,0}$ are negligible for Reynolds numbers greater than about 7500.

The above conditions ensure the satisfaction of local and global flux conservation, boundary conditions, and all other relevant physical requirements. We are now free to impose any other physically realistic condition to close the system. The number of conditions needed is $N_i(N_j - 1) - N_a$. This is precisely the number of horizontal interfaces in the mesh (minus those that coincide with the airfoil). Consequently, there is an additional degree of freedom in specifying horizontal interface conditions. For the present problem, we require the u velocity to be continuous at the midpoint of each horizontal interface.

By virtue of conditions (3.3), there are 16 unknowns on each solution element. However, using the local constraints (2.56), (2.59), (2.63), (2.91), (2.92), and (2.96), six of the unknowns may be eliminated in terms of other variables. The total number of unknowns that must be explicitly solved for is then $10N_iN_j$.

The discrete boundary value problem outlined above is a coupled system of second-order polynomial equations in the unknown coefficients $u_{0,0}$, $v_{0,0}$, $p_{0,0}$, etc.. Our experience has shown that this system may be solved very efficiently using Newton's method.

In what follows, we discuss numerical results for high-Reynolds-number flow (Re = 100,000) around a finite flat plate. Previous efforts to solve the full Navier-Stokes equations for the flat plate problem have usually involved a vorticity-stream function formulation (Dennis et al, 1965; McLachlan, 1991). To our knowledge, no solutions to the full Navier-Stokes equations have yet been published for Reynolds numbers higher than about 4000. McLachlan (1991) has reported some of the numerical difficulties that are encountered as the Reynolds number approaches 4000. On the other hand, as we stated above, our assumption (3.3) becomes invalid for Reynolds numbers less than about 7500. As a result, no direct comparison with vorticity-stream function results can be made at this time. However, at the very high Reynolds number of 100,000, we may compare with the analytical solutions of Blasius (1908) and Goldstein (1929) to assess the accuracy of our results.

The Blasius solution may also be used as a guide for constructing a mesh for numerical calculations. If we let Re denote the Reynolds number based on the airfoil chord c, then the similarity relation (Schlicting, 1979; White, 1974)

$$\eta = y\sqrt{\frac{U}{2\nu x}} \tag{3.4}$$

becomes

$$\eta = \sqrt{Re}\,\frac{y}{c}\sqrt{\frac{U/U_\infty}{2(\nu/\nu_\infty)(x/c)}} \tag{3.5}$$

where all quantities except η and Re are dimensional. Identifying the free-stream velocity U with U_∞, and assuming constant viscosity, equation (3.5) becomes

$$\eta = \sqrt{Re}\,\frac{y}{c}\sqrt{\frac{c}{2x}}. \tag{3.6}$$

Corresponding to any η, x and y are related through the equation

$$\frac{y}{c} = \eta\sqrt{\frac{2}{Re}}\,\sqrt{\frac{x}{c}}. \tag{3.7}$$

Equation (3.7) allows us to estimate the location of the edge of the boundary layer for any fixed $\frac{x}{c}$. We take $\eta = 6.0$, corresponding to $\frac{U}{U_\infty} = 0.999999$, (White, 1974) to be the edge of the boundary layer. An estimate of the boundary layer thickness δ_x at any $\frac{x}{c}$ is then given by

$$\delta_x = 6.0\sqrt{\frac{2}{Re}}\,\sqrt{\frac{x}{c}}. \tag{3.8}$$

At the trailing edge we have the estimate

$$\delta_{t.e.} = 6.0\sqrt{\frac{2}{Re}}. \tag{3.9}$$

When Re = 100,000, one gets $\delta_{t.e.} = 0.0268$. The free-stream mesh boundaries may then be taken to be $y = \pm 0.027$. Similarly, at the leading edge, say $\frac{x}{c} = .01$, the estimated boundary layer thickness is $0.00268 \approx 0.0027$. An estimate for Δy is then $0.0027/\mathrm{N}_{l.e.}$, where $\mathrm{N}_{l.e.}$ is the number of cells required to resolve the leading edge boundary layer. If $\mathrm{N}_{l.e.} = 2$, one obtains $\Delta y = .00135$. (Recall that the present discretization represents u quadratically. See (2.13).)

Unlike the free-stream boundaries, the upstream and downstream boundaries may be located somewhat arbitrarily. For the present study, we take the upstream boundary to be $x = -0.1$, and the downstream boundary to be $x = 1.5$.

Newton's method has proven to be a robust solution technique for the present discretization. Our experience has shown that an initial guess of uniform flow is usually sufficient to ensure convergence. However, convergence problems have been observed for certain mesh spacings and grid aspect ratios. In Figure 4 we show the results of a systematic study which was performed to determine the scheme's domain of convergence at Re = 100,000. For purposes of the study, we limited the number of solution elements in the x direction to 400, and in the y direction to 60. This corresponds to minimum x and y spacings of $\frac{1}{250} = 0.004$ and $\frac{.027}{30} = 0.0009$, respectively. The mesh boundaries were held

fixed at $y = \pm 0.027$, $x = -0.1$, and $x = 1.5$. The scheme is stable and convergent on the boundary and interior of the region shown in Figure 4. The scheme remains stable and convergent to the exterior of the dashed portion of the boundary, but becomes unstable and/or nonconvergent to the exterior of the solid boundary. (We should point out that when we used symmetry to solve for only the upper half flow field, the scheme was unstable for all mesh spacings. Apparently, the instability was caused by the leading edge singularity, which invalidated our symmetry boundary condition.)

Using our earlier estimate $\Delta y = .00135$ for the y mesh spacing, along with the fixed grid boundaries described above, we obtain a baseline grid by choosing a grid aspect ratio $r = \frac{\Delta y}{\Delta x}$. Taking $r = .155$, we obtain a baseline 185 x 40 grid with $\Delta x = .0087$.

For flat plate flow at high Reynolds numbers, it is well known that the Blasius solution provides the correct boundary layer profile over a substantial part of the airfoil. Stewartson (1969) and Messiter (1970) have shown that the Blasius solution remains valid to within an $O(Re^{-\frac{3}{8}})$ region near the trailing edge. On the other hand, near the leading edge, the Blasius solution is not valid but becomes valid as Re_x (Reynolds number based on distance from leading edge) becomes large (Jones et al, 1988).

Figure 5 shows how our Navier-Stokes solution differs from the Blasius solution for a series of calculations that were performed on successively finer grids. The coarsest mesh is the baseline grid described above. Each succesive grid is refined by adding four cells in the y direction and holding r constant at .155. The finest grid is 313 x 68 with $\Delta y = .000794$, $\Delta x = \frac{1}{195} = .00513$, and $r = .15485$. The figure shows $\|u_{0,0} - u_B\|_\infty = \max_j |u_{0,0} - u_B|$ as a function of x for the full length of the airfoil, where u_B is the Blasius streamwise velocity. The results indicate that our Navier-Stokes solution and the Blasius boundary layer solution are in closest agreement at around $x = .75$, the three-quarter chord point.

In Figures 6 and 7, using results from the baseline and 313 x 68 grids, we compare $u_{0,0}$ and $v_{0,0}$ with their analytical counterparts at $x = .25, .5$, and $.75$. The results obtained from the finest mesh clearly show excellent agreement for both $u_{0,0}$ and $v_{0,0}$. At $x = .75$, the maximum difference between $u_{0,0}$ and u_B is .00157. If we take u_B to be the exact solution, we find the maximum relative error of $u_{0,0}$ to be .0032 at $x = .75$. For the baseline grid, we find a maximum absolute error of .00486, and a maximum relative error of .0265. Based on these results, we estimate that the fine grid calculation is in error by less than .32%, and the baseline grid is in error by less than 2.7%.

We now examine the rate at which the error (i.e., $\|u_{0,0} - u_B\|_\infty$ at $x = .75$) is reduced with mesh refinement. Figure 8 shows the effect of refining in the x direction while Δy is held constant. Surprisingly, the results show that x grid refinement at constant Δy (i.e., increasing the grid aspect ratio) leads to an *increase* in the error. As Δy decreases, this effect becomes stronger. Figure 9 shows a log-log plot of the error versus r. The slopes for the four cases are .156, .230, .310, and .390.

It follows from the above that mesh refinement in the y direction must be done at constant r if we wish to determine how the error is reduced with Δy. Figure 10 compares the error from 148 x 32 and 296 x 64 grids with r fixed at .15525. The maximum error is

.007118 and .001754, respectively, so that the error is reduced by a factor of 4.06.

Figure 11 shows a log-log plot of the error versus Δy for five grids with $r = .15525$. The fine-grid to coarse-grid slope is 2.02. The four intermediate slopes are, from left to right, 1.84, 2.24, 2.35, and 1.71, for an average slope of 2.035. The reduction in error is thus second order in Δy.

The above results imply that the error decreases like $r^{\alpha}\,\Delta y^2$ where, roughly, $0.156 \leq \alpha \leq 0.390$. Mesh refinement at constant Δx confirms that this is the case. Refining a 296 x 32 grid to a 296 x 64 grid reduces both r and Δy by a factor of two. Taking $\alpha = .156$, one predicts that the error will be reduced by a factor of $(2^{0.156})(2^2) = 2^{2.156} = 4.457$. From numerical calculations we obtain an error reduction factor of $\frac{.007913}{.001754} = 4.511$, which corresponds to $\alpha = 0.174$. Similarly, refining a 296 x 56 grid to 296 x 64, one predicts that the error will be reduced by a factor ranging from $(\frac{8}{7})^{2.156} = 1.334$ to $(\frac{8}{7})^{2.39} = 1.376$. From numerical calculations we find that the error is reduced by a factor of $\frac{.002422}{.001754} = 1.381$, which corresponds to $\alpha = 0.417$. The above results are summarized in Table 1, along with additional results. We find that α assumes an average value of 0.247. The one anomalous result, where α = -.395, results from an unusually favorable accuracy on the 313 x 60 grid, as is evidenced by the last case shown in the table, where $\alpha = .586$.

We now present numerical results for the pressure coefficient, coefficient of friction, and wake velocity (from the 313 x 68 grid described above). The trailing edge pressure singularity shown in Figure 12 indicates that C_p assumes a minimum value of $-.0149$. This compares well with the results of Srinivasan et al (1992), who studied flat plate trailing edge flow at Re = 100,000 using a reduced Navier-Stokes (RNS) scheme.

The results shown in Figure 13 indicate that our Navier-Stokes C_f is slightly larger than the Blasius C_f $(C_f(B) = \frac{.6641}{\sqrt{Re\,x}})$ near the trailing edge. This agrees with the findings of a number of researchers who have derived second-order corrections to the Blasius drag (Kuo, 1953; Imai, 1964; Stewartson, 1969; Messiter, 1970). Near the leading edge, our results show a small decrease in C_f which continues up to $x = .0231$. The net result is that the increase in C_f near the trailing edge is more than cancelled by the decrease at the leading edge, and we obtain a drag coefficient of .004171 which is 99.31% of the Blasius value of .004200 $= \frac{1.3282}{\sqrt{Re}}$.

In Figure 14 we compare with Goldstein's (1929) wake solution. The solid lines in the figure are our Navier-Stokes solution. They were generated using the full functional representation of u on each cell (see 2.13). The diamond-shaped symbols represent the numerical solution at the cell center (i.e., $u_{0,0}$), whereas the squares are Goldstein's solution. (For accuracy reasons we limited the comparison to points where Goldstein's η was less than or equal to .75.) The results show that the agreement is not very good until around x = 1.15. This is consistent with triple deck theory, which has shown that Goldstein's wake solution is not valid in an $O(Re^{-\frac{3}{8}})$ region near the trailing edge. It is clear, however, that our numerical results do not agree nearly as well with the Goldstein wake solution as they do with the Blasius flat plate solution. This can be attributed to the fact that the Goldstein solution is an asymptotic solution to the boundary layer equations, whereas the

Blasius solution is an exact solution (admittedly obtained by numerical means).

We conclude with a discussion of results from nonuniform grids. Since the entire discretization presented in Section II remains valid if Δx and Δy are replaced by Δx_i and Δy_j, respectively, application of our scheme to variably-spaced grids is straightforward.

The results shown in Figures 15 and 16 are taken from fine and coarse grids, respectively. The fine grid is 240 x 40 with 4.1% exponential y stretching and has Δy(wall) $\stackrel{def}{=} \Delta y_w = .0009$. The coarse grid is 112 x 20 with 14.7% exponential y stretching and $\Delta y_w = .00135$. The solid lines in the figures are obtained using the full functional solution for the u velocity, and the diamonds correspond to values of $u_{0,0}$. Comparison is made with both the Blasius and Goldstein solutions. The accuracy of the fine grid solution is comparable to that of the finest uniform grids considered above, and the accuracy of the coarse grid solution is comparable to that of the baseline 185 x 40 mesh. We obtain drag coefficients $C_D = .004166$ from the fine grid and $C_D = .004124$ from the coarse grid. Based on our earlier drag results, we estimate that these values are in error by less than .4% and 1.4%, respectively. Both computations converged in eight Newton iterations, starting from uniform flow, to a maximum residual error which is less than 1.2×10^{-10}. The CPU times on a Cray YMP were 580 seconds for the fine grid and 50 seconds for the coarse grid. These times would be reduced by about 15% if our code was optimized for computational efficiency instead of storage efficiency.

Finally, we should mention that numerical stability for nonuniform grids depends rather strongly on the wall grid aspect ratio, $r_w = \frac{\Delta y_w}{\Delta x}$. Our experience has shown that the domain of convergence in Figure 4 very nearly provides the domain of convergence for stretched grids if one replaces r and Δy with r_w and Δy_w, respectively.

Concluding Remarks

The numerical results presented above have clearly shown an accurate resolution of the flat plate flow field. We showed in particular that the streamwise velocity is obtained to order $r^\alpha \Delta y^2$, where $\alpha \approx 0.25$. In a future paper we will perform a similar analysis to determine the order of accuracy of the discrete derivatives.

Finally, the effort to generalize the discretization presented in this paper is ongoing. We recently presented (Scott et al, 1995) a methodology for retaining all the discrete unknowns in the local expansions, and extended the discretization to quadralateral conservation elements of arbitrary shape. Numerical results obtained to date would seem to indicate that the present approach offers significant potential to resolve laminar boundary layers on relatively coarse grids with only moderate computational effort.

References

Anderson, D.A., Tannehill, J.C., and Pletcher, R.H. (1984) *Computational Fluid Mechanics and Heat Transfer*, (Hemisphere), 190-193.

Buck, R.C. (1978) *Advanced Calculus*, 3rd. ed., International Series in Pure and Applied Mathematics, Spanier, E.H., Springer, G., and Davis, P.J., Consulting Eds., (McGraw-Hill), 152.

Chang, S.C. (1995) "The Method of Space-Time Conservation Element and Solution Element – A New Approach for Solving the Navier-Stokes and Euler Equations," *J. Comp. Phys.*, **119**, 295-324.

Dennis, S.C.R. and Dunwoody, J. (1965) "The Steady Flow of a Viscous Fluid Past a Flat Plate," *J. Fluid Mech.*, **24**, 3, 577-595.

Goldstein, S. (1929) "Concerning Some Solutions of the Boundary Layer Equations in Hydrodynamics," *Proc. Cambridge Philos. Soc.*, **26**, 1, 1-30.

Imai, I. (1964) "On the Viscous Flow Near the Trailing Edge of a Flat Plate," *Proc. XI International Congress of Applied Mechanics*, H. Görtler, Ed., Springer-Verlag, Berlin, 663-671.

Jones, C.W. and Watson, E.J. (1988) "Two-Dimensional Boundary Layers," in *Laminar Boundary Layers*, L. Rosenhead, Ed., (Dover Publications, Inc.), 226-227.

Kuo, Y.H. (1953) "On the Flow of an Incompressible Viscous Fluid Past a Flat Plate at Moderate Reynolds Numbers," *J. Math. Phys.*, **32**, 83-101.

McLachlan, R.I. (1991) "The Boundary Layer on a Finite Flat Plate," *Phys. Fluids*, A, **3**, 2, 341-348.

Messiter, A.F. (1970) "Boundary-Layer Flow Near The Trailing Edge of a Flat Plate," *SIAM J. Appl. Math.*, **18**, 1, 241-257.

Schlichting, H. (1979) *Boundary-Layer Theory*, 7th. ed., McGraw-Hill Series in Mechanical Engineering, Holman, J.P., Consulting Ed., (McGraw-Hill), 135-140.

Scott, J.R. and Chang, S.C. (1995) "A New Flux-Conserving Newton Scheme for the Navier-Stokes Equations," *IJCFD*, **5**, 189-212. (First published as "A New Flux Conserving Newton's Method Scheme for the Two-Dimensional, Steady Navier-Stokes Equations," NASA TM 106160, 1993.)

Scott, J.R. and Chang, S.C. (1995) "The Space-Time Solution Element Method – A New Numerical Approach for the Navier-Stokes Equations," AIAA-95-0763, NASA TM 106818.

Srinivasan, K. and Rubin, S.G. (1992) "Segmented Multigrid Domain Decomposition Procedure For Incompressible Viscous Flows", *International Journal For Numerical Methods in Fluids*, **15**, 1333-1355.

Stewartson K. (1969) "On the Flow Near the Trailing Edge of a Flat Plate," II, *Mathematika*, **16**, 106-121.

White, F.M. (1974) *Viscous Fluid Flow*, (McGraw-Hill), 261-266.

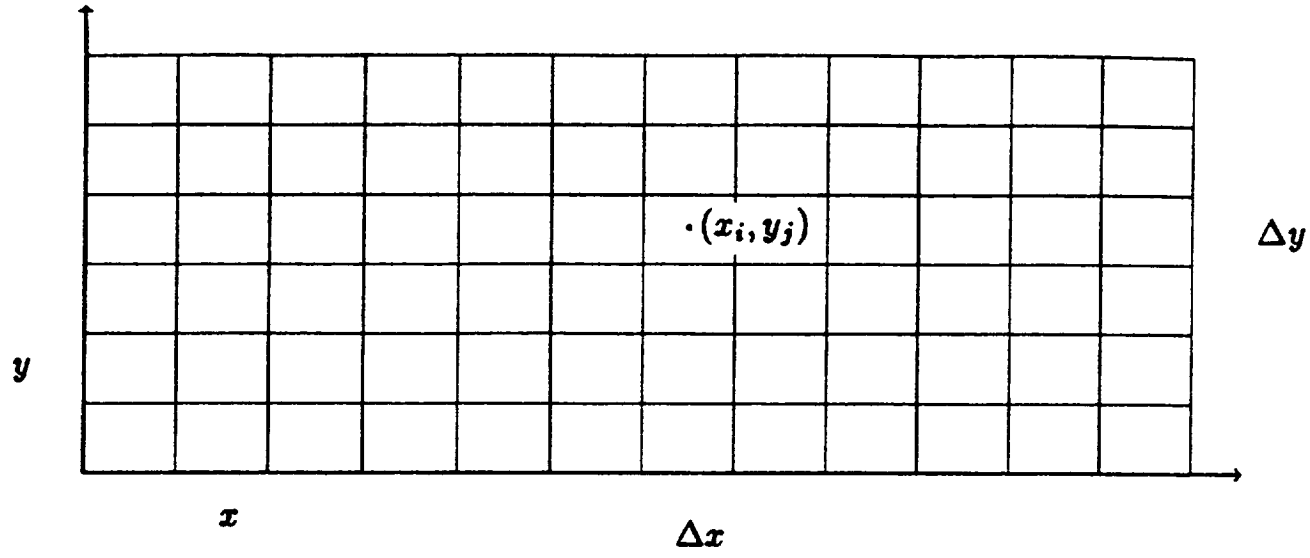

Figure 1 Discretization of E_2.

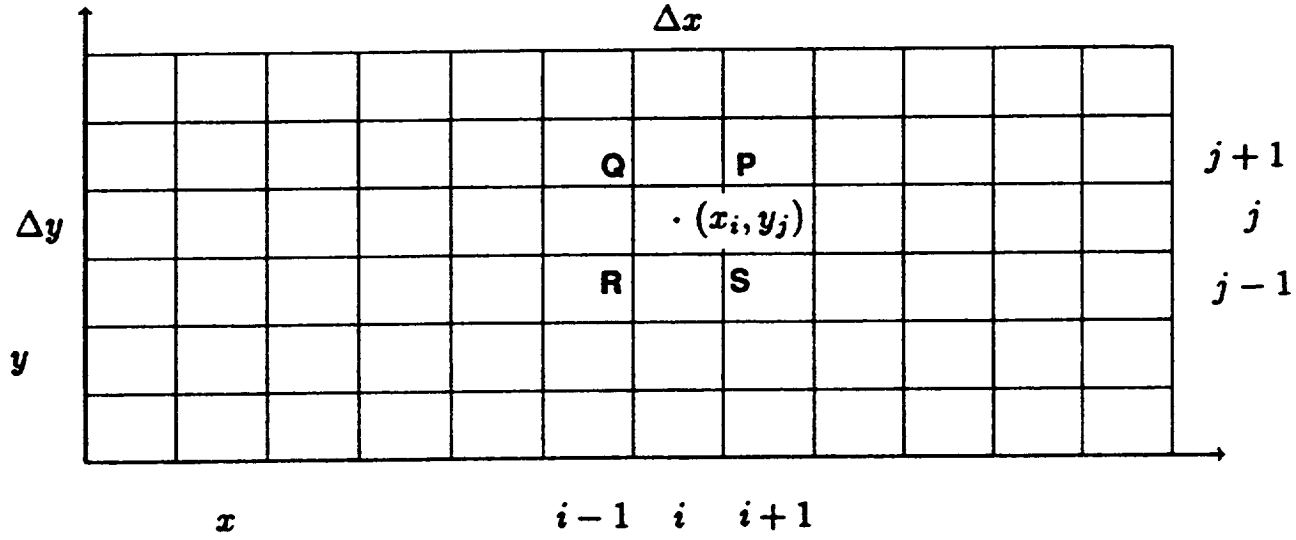

Figure 2 Orientation for Line Integration Around S(CE(i,j)).

Figure 3 Computational grid for a finite flat plate. The airfoil lies on the x-axis between x = 0 and x = 1.

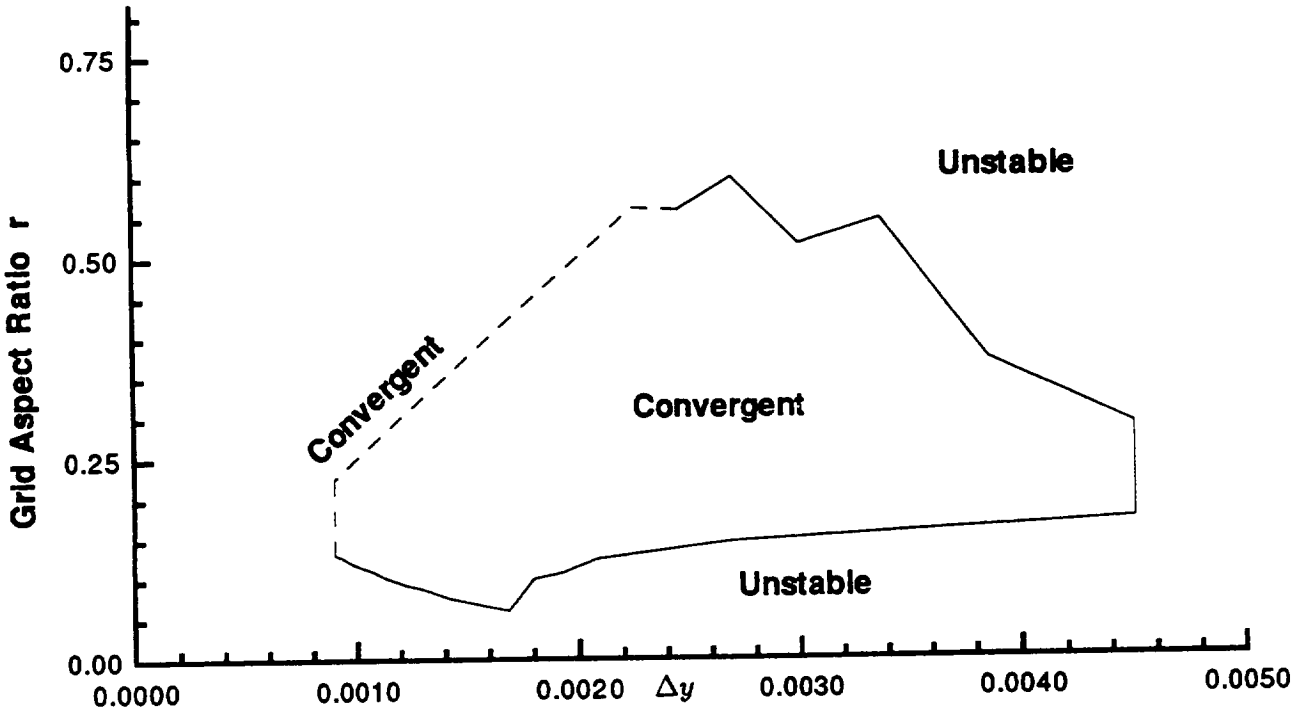

Figure 4 Domain of convergence for a finite flat plate at Re = 100,000. The scheme is convergent on the interior and boundary of the enclosed region, and remains convergent to the exterior of the dashed boundary.

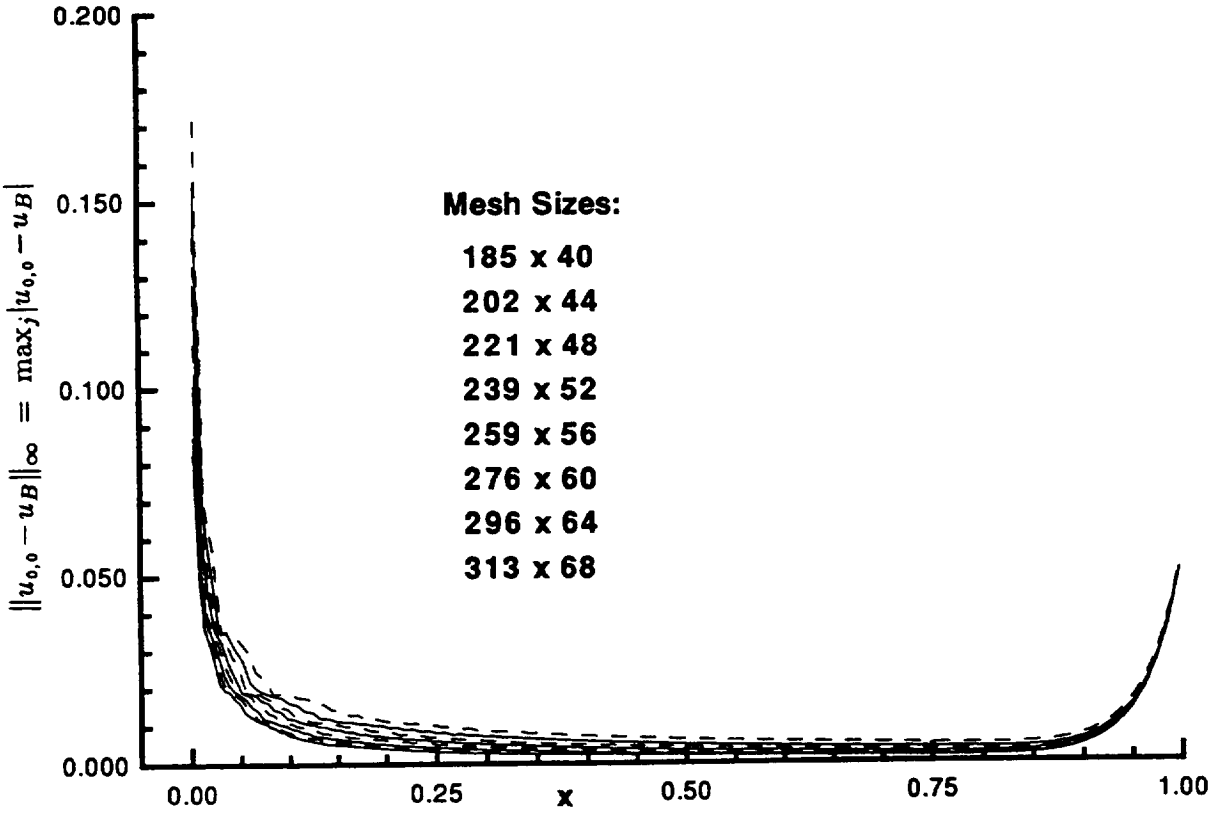

Figure 5 Maximum deviation of Navier-Stokes solution from Blasius solution at Re = 100,000 for eight different calculations. Grid aspect ratio = .155.

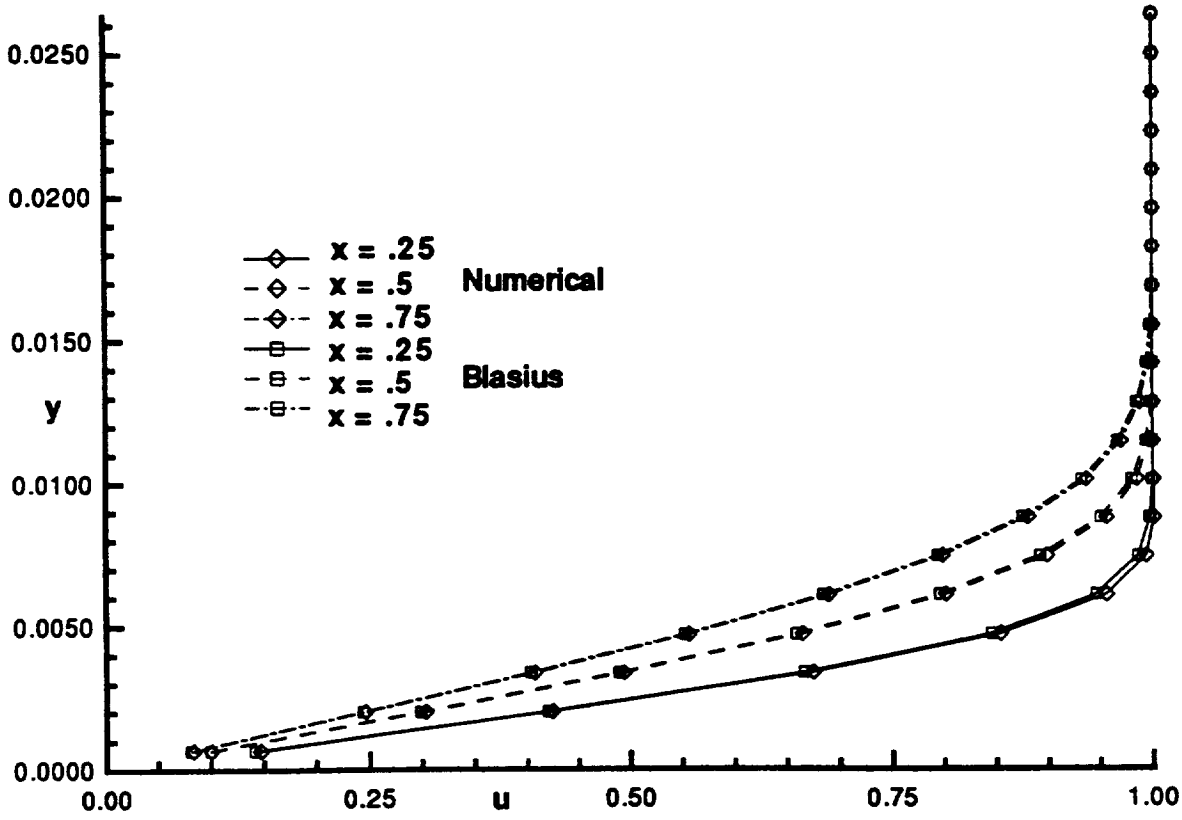

Figure 6a Comparison of predicted u velocity with Blasius solution at x = .25, .5, and .75. 185 x 40 Baseline Grid. Re = 100,000.

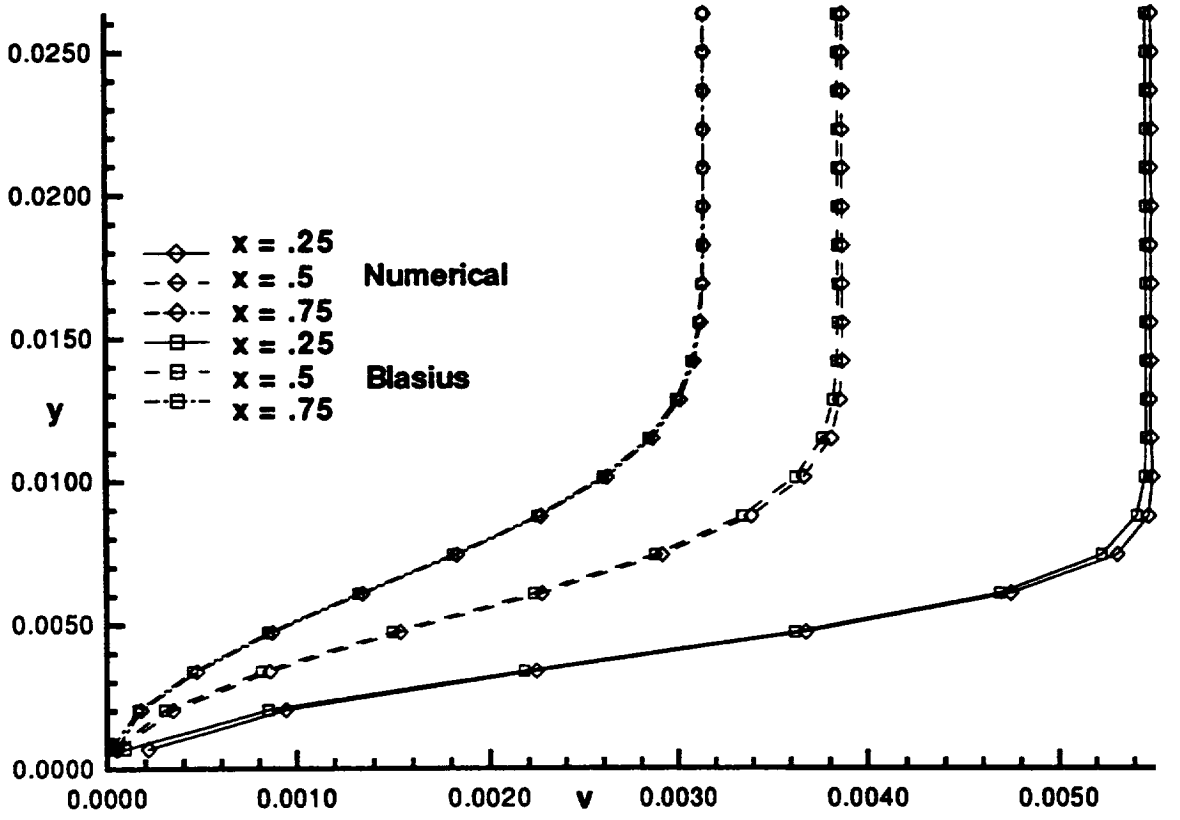

Figure 6b Comparison of predicted v velocity with Blasius solution at x = .25, .5, and .75. 185 x 40 Baseline Grid. Re = 100,000.

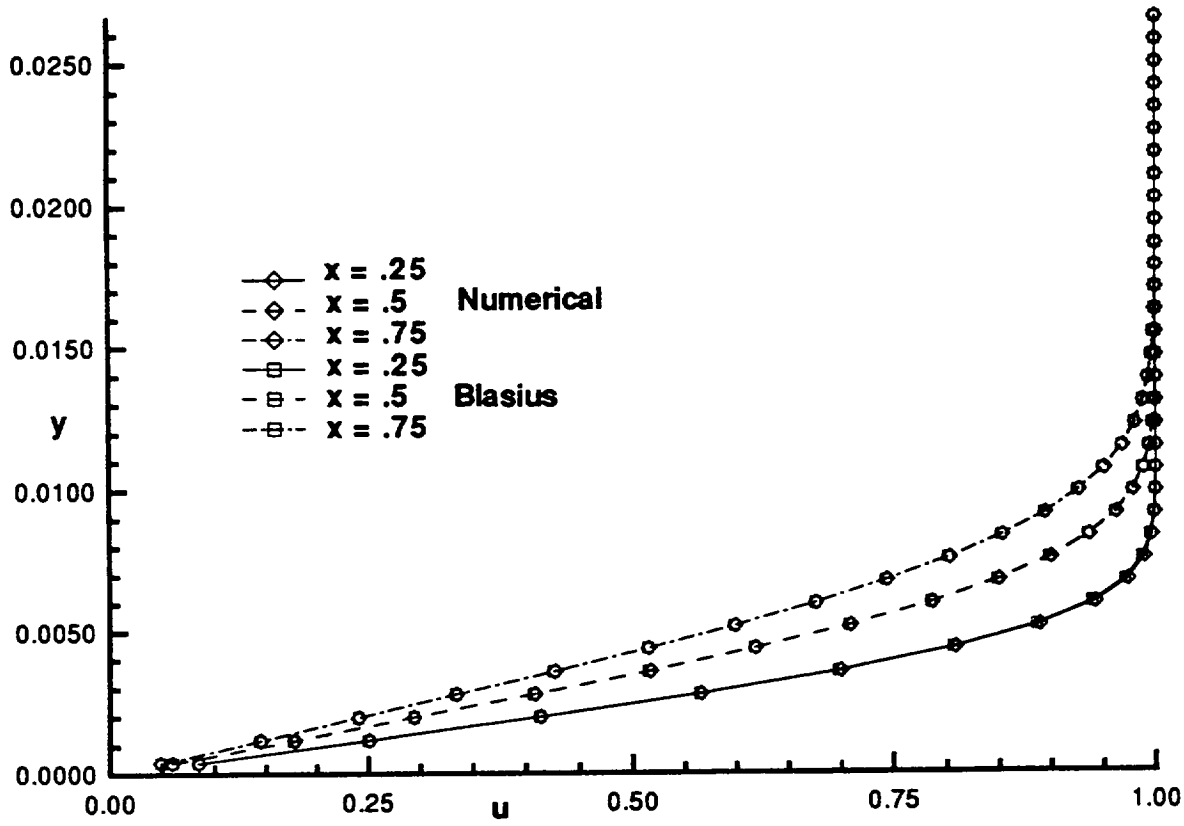

Figure 7a Comparison of predicted u velocity with Blasius solution at x = .25, .5, .75. 313 x 68 Fine Grid. Re = 100,000.

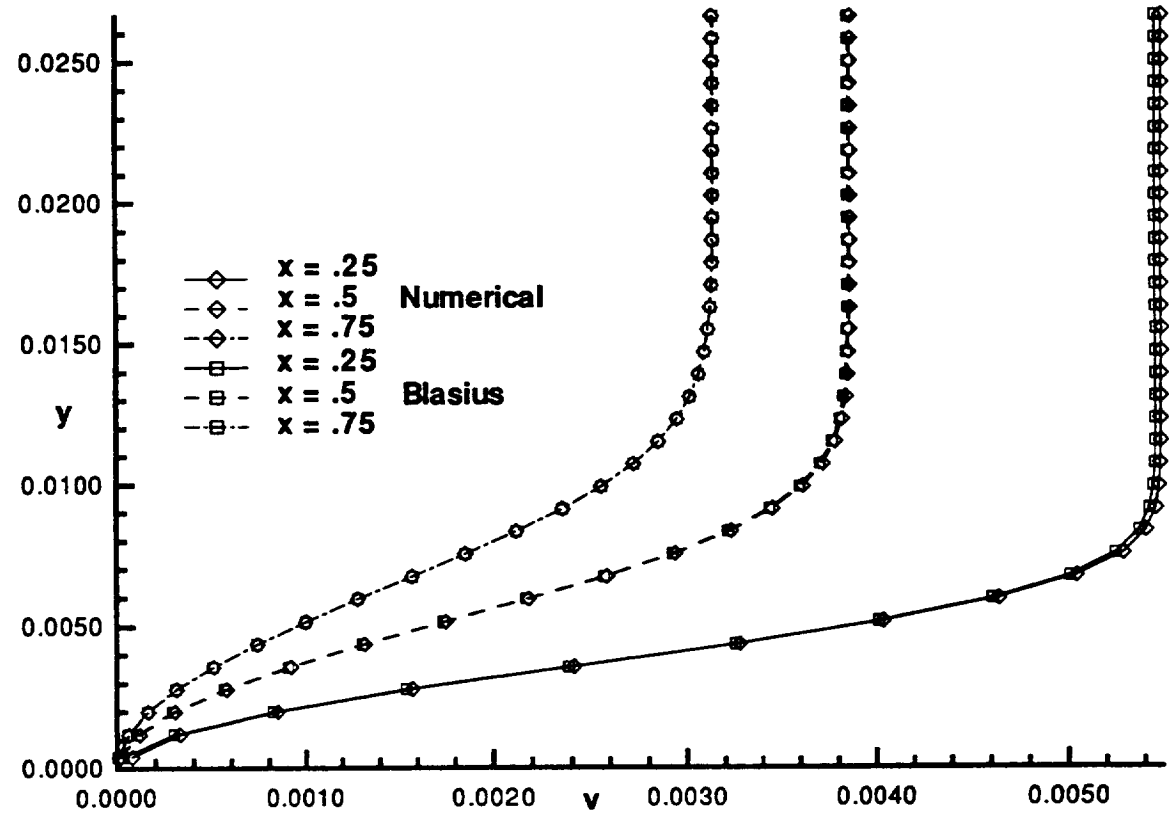

Figure 7b Comparison of predicted v velocity with Blasius solution at x = .25, .5, .75. 313 x 68 Fine Grid. Re = 100,000.

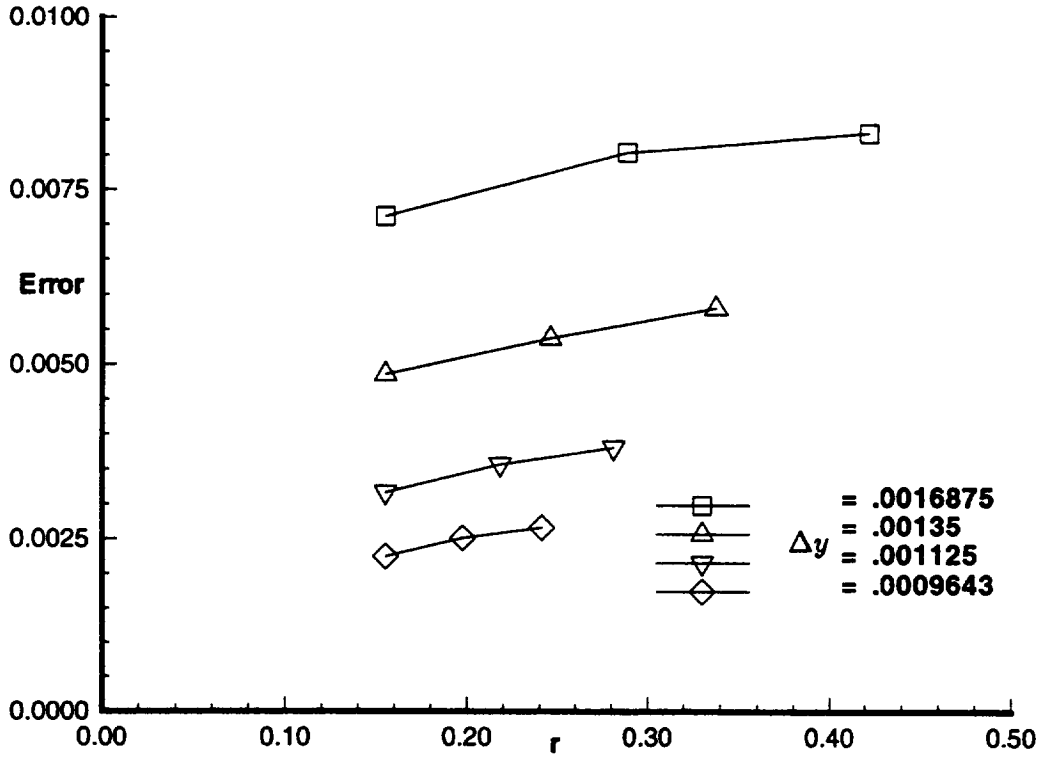

Figure 8 Effect of grid aspect ratio on accuracy for four different values of Δy .

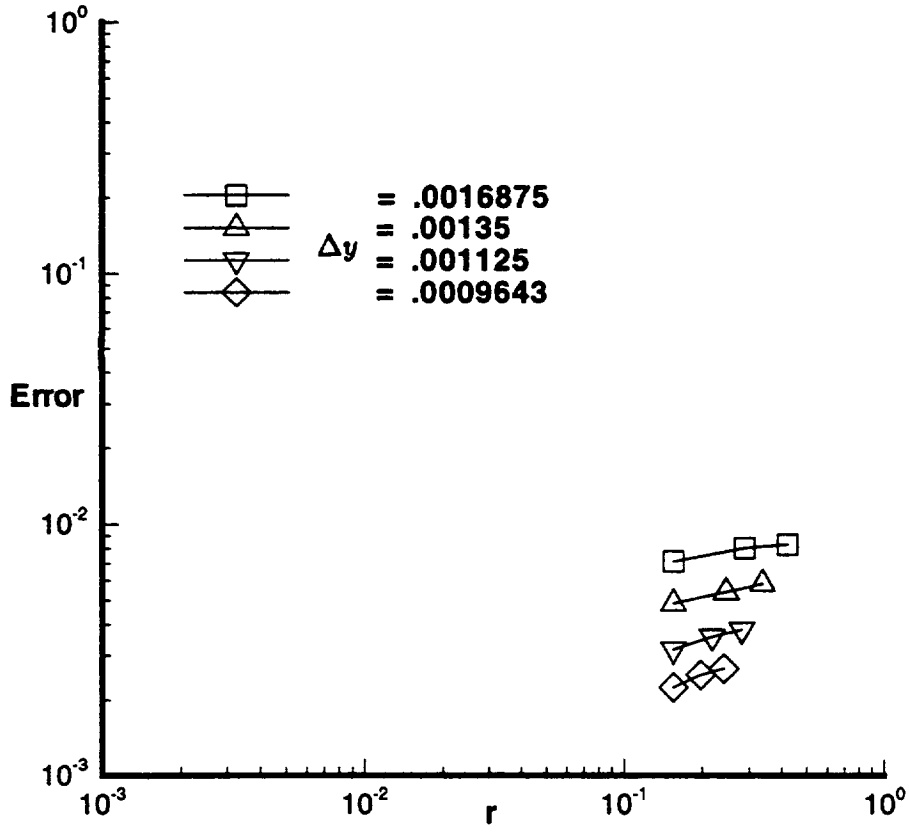

Figure 9 Effect of grid aspect ratio on accuracy for four different values of Δy . The slopes are, from top to bottom, .156, .230, .310, and .390, respectively.

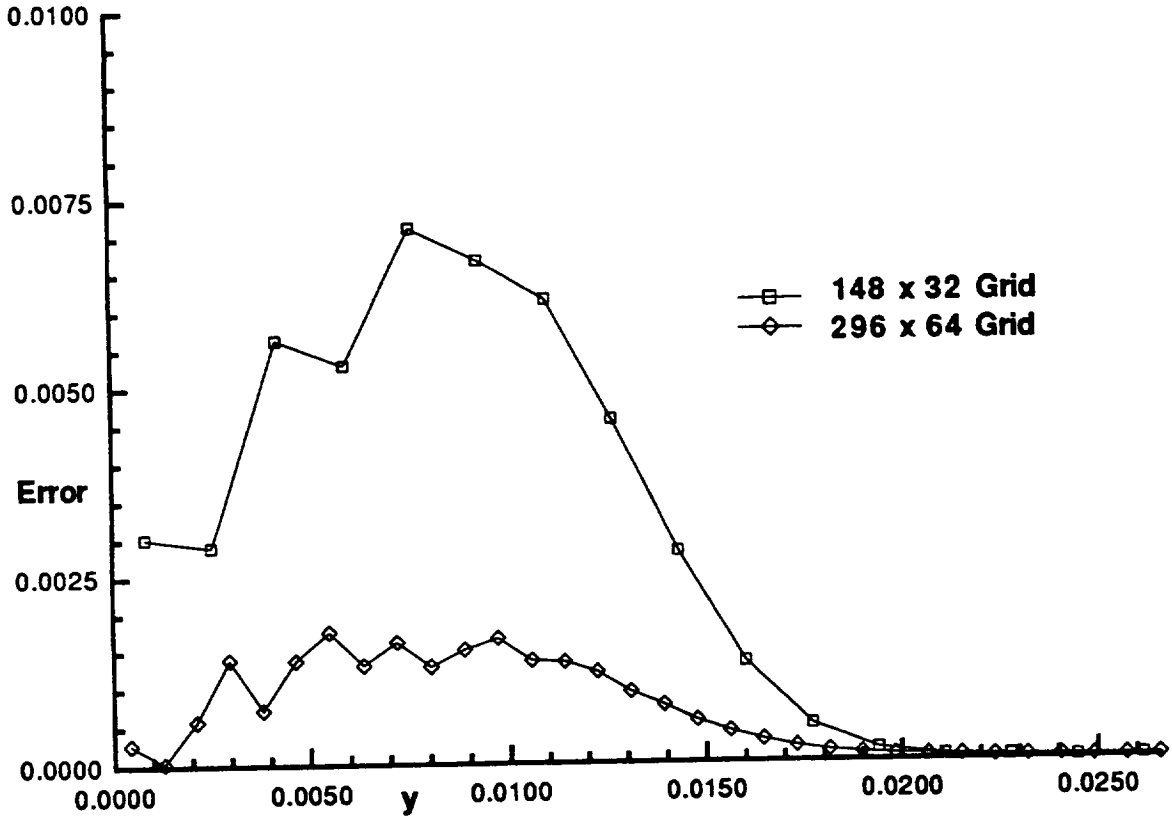

Figure 10 Comparison of numerical error at x = .75 for 148 x 32 and 296 x 64 grids with r = .15525. Max error = .007118 and .001754, respectively.

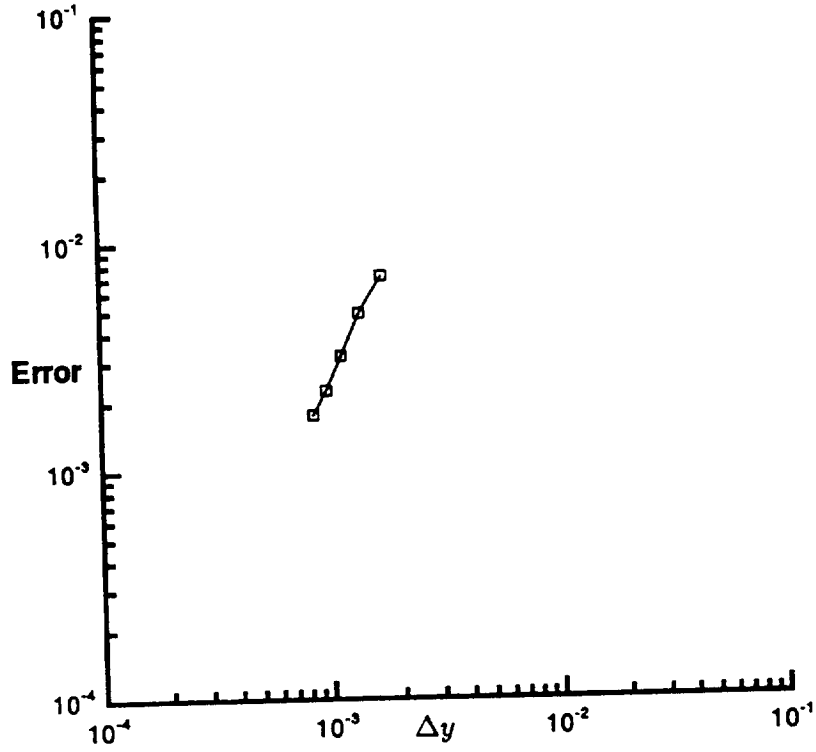

Figure 11 Reduction in error at x = .75 due to mesh refinement at constant grid aspect ratio r = .15525. Grid sizes = 148 x 32, 185 x 40, 221 x 48, 259 x 56, and 296 x 64.

Grid Refinement	Error Ratio $= e_1/e_2$	$\log(e_1/e_2)/\log(\Delta y_1/\Delta y_2)$	α
296 x 32 to 296 x 64	$\frac{.007913}{.001754} = 4.511$	2.174	0.174
296 x 40 to 296 x 64	$\frac{.005497}{.001754} = 3.134$	2.430	0.430
296 x 48 to 296 x 64	$\frac{.003481}{.001754} = 1.985$	2.383	0.383
296 x 56 to 296 x 64	$\frac{.002422}{.001754} = 1.381$	2.416	0.416
313 x 36 to 313 x 68	$\frac{.006341}{.001573} = 4.031$	2.192	0.192
313 x 44 to 313 x 68	$\frac{.004292}{.001573} = 2.729$	2.306	0.306
313 x 52 to 313 x 68	$\frac{.002784}{.001573} = 1.770$	2.128	0.128
313 x 60 to 313 x 68	$\frac{.001923}{.001573} = 1.223$	1.605	-0.395
313 x 52 to 313 x 60	$\frac{.002784}{.001923} = 1.448$	2.586	0.586

Table 1 Grid refinement at constant Δx. $\alpha_{avg} = .247$

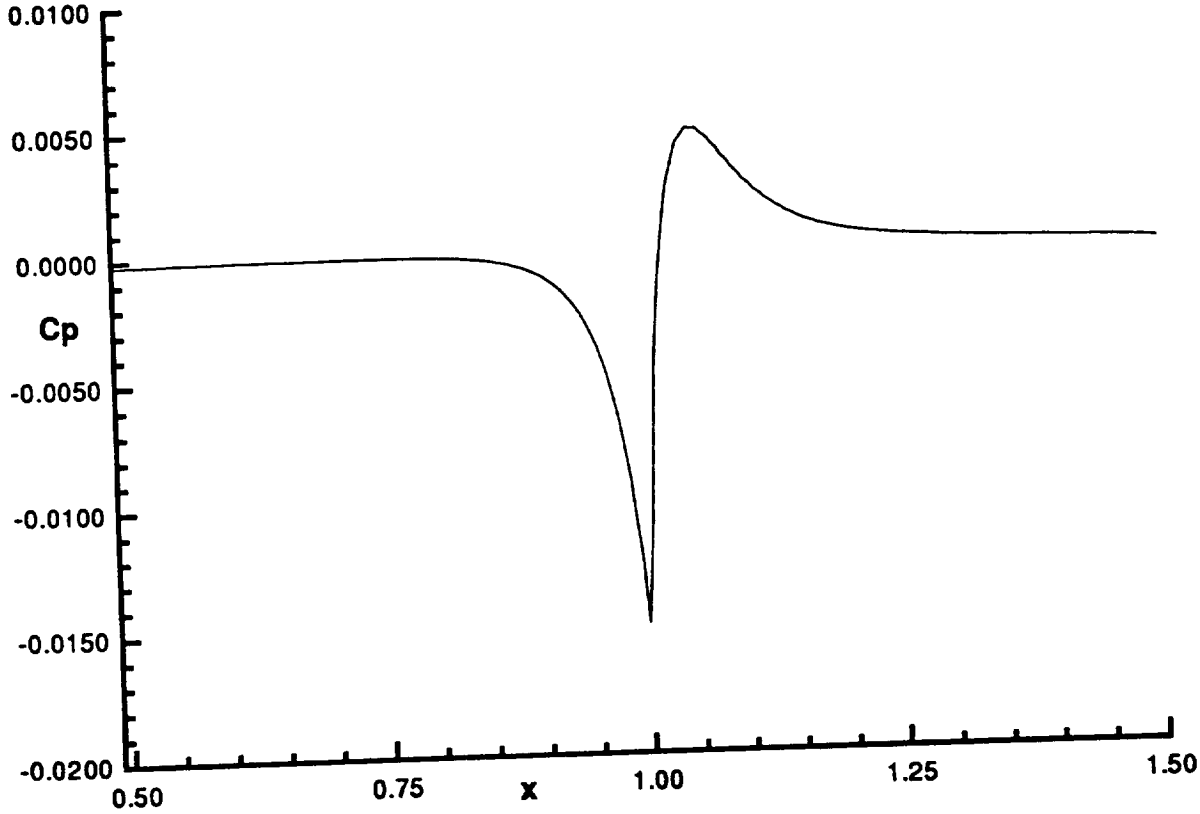

Figure 12 Pressure coefficient in the trailing edge region. Re = 100,000. 313 x 68 Grid.

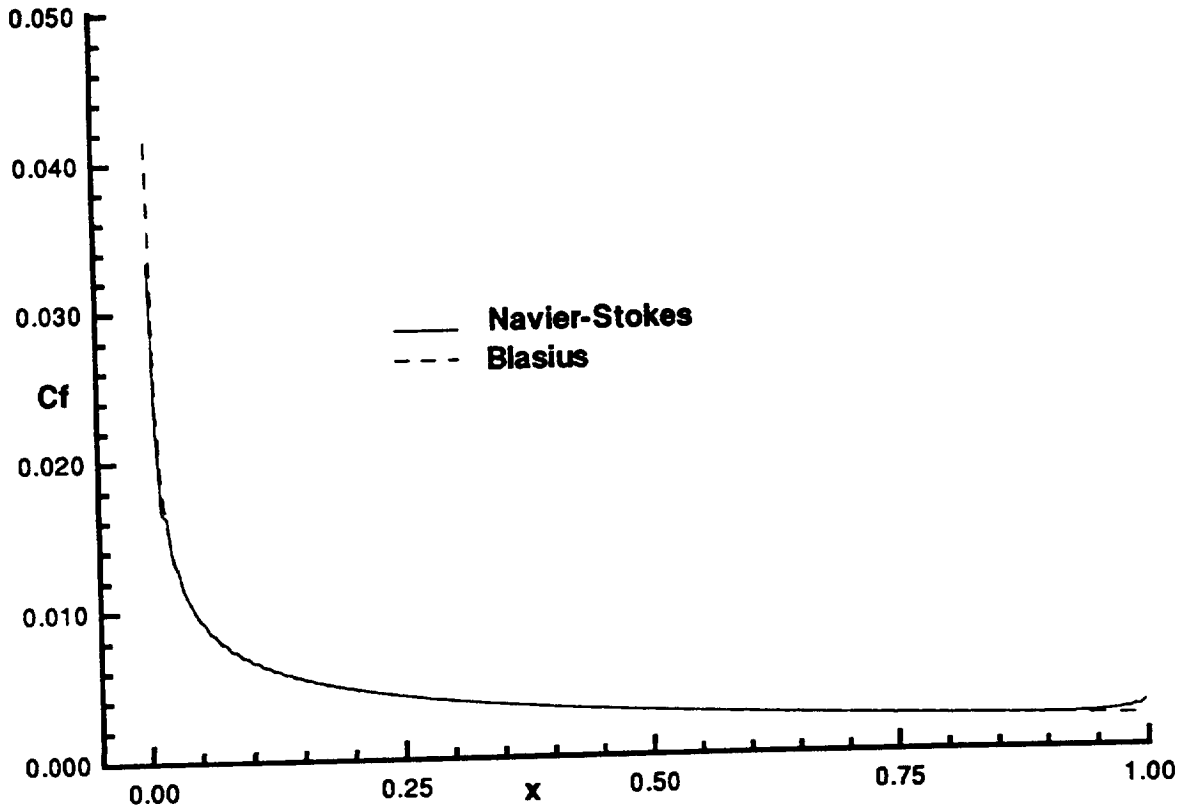

Figure 13 Comparison of coefficient of friction from computed Navier-Stokes solution versus Blasius Cf at Re = 100,000. 313 x 68 Grid.

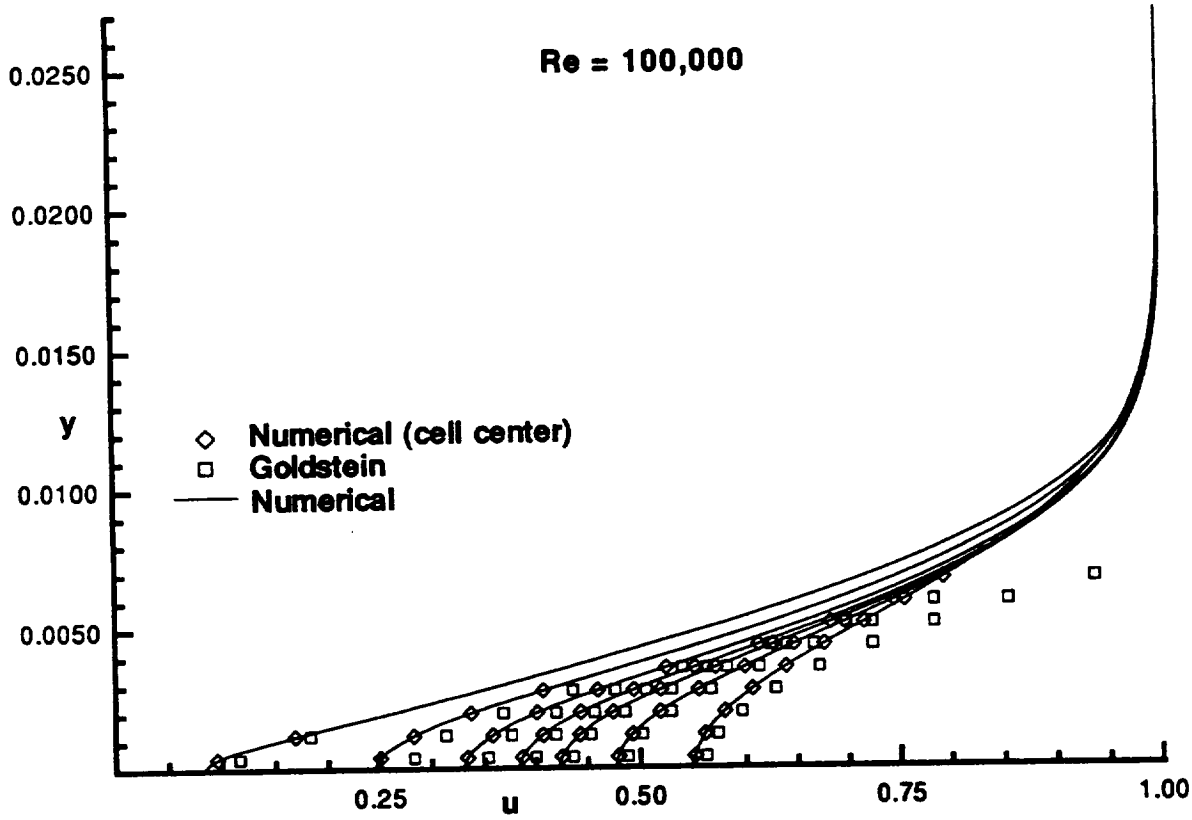

Figure 14 Comparison of predicted u velocity with Goldstein wake solution at x = 1.00256, 1.04872, 1.1, 1.15128, 1.20256, 1.3, and 1.5. 313 x 68 Grid.

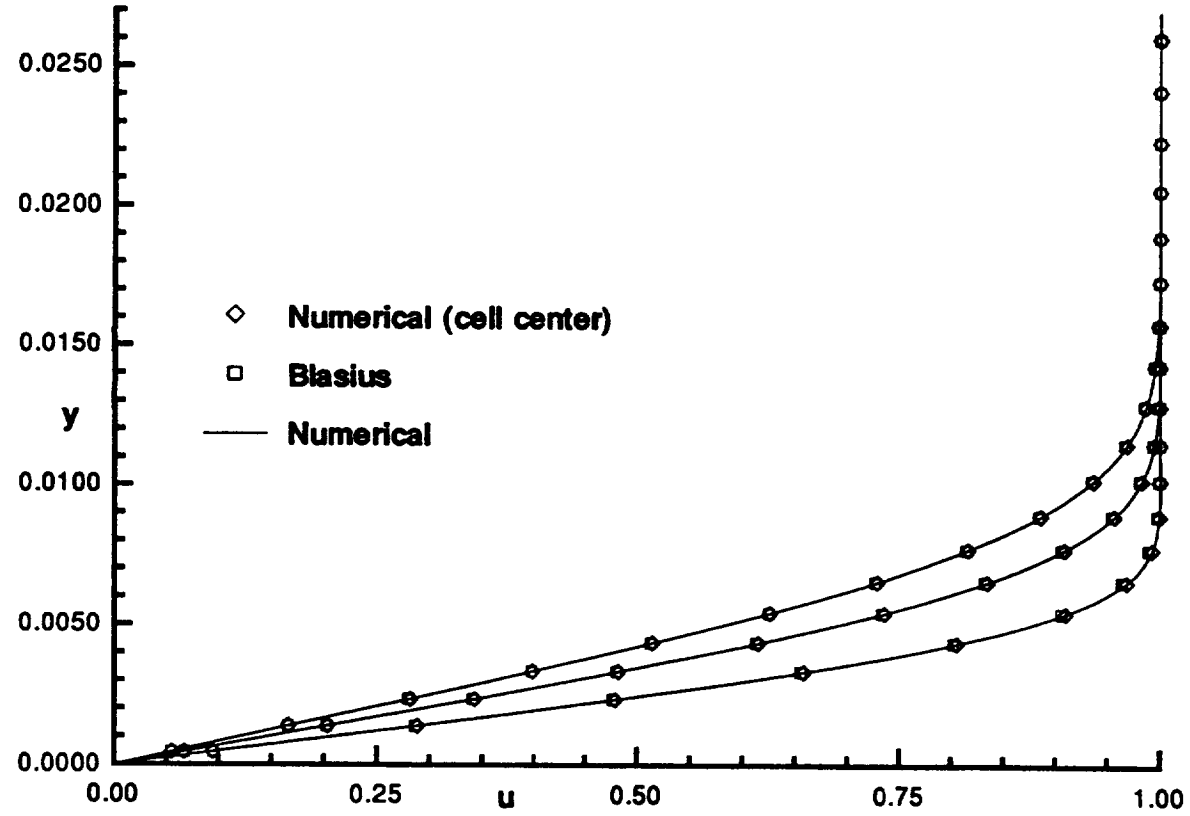

Figure 15a Comparsion of predicted u velocity with Blasius solution at x = .25, .5, .75. 240 x 40 Stretched Grid. Re = 100,000.

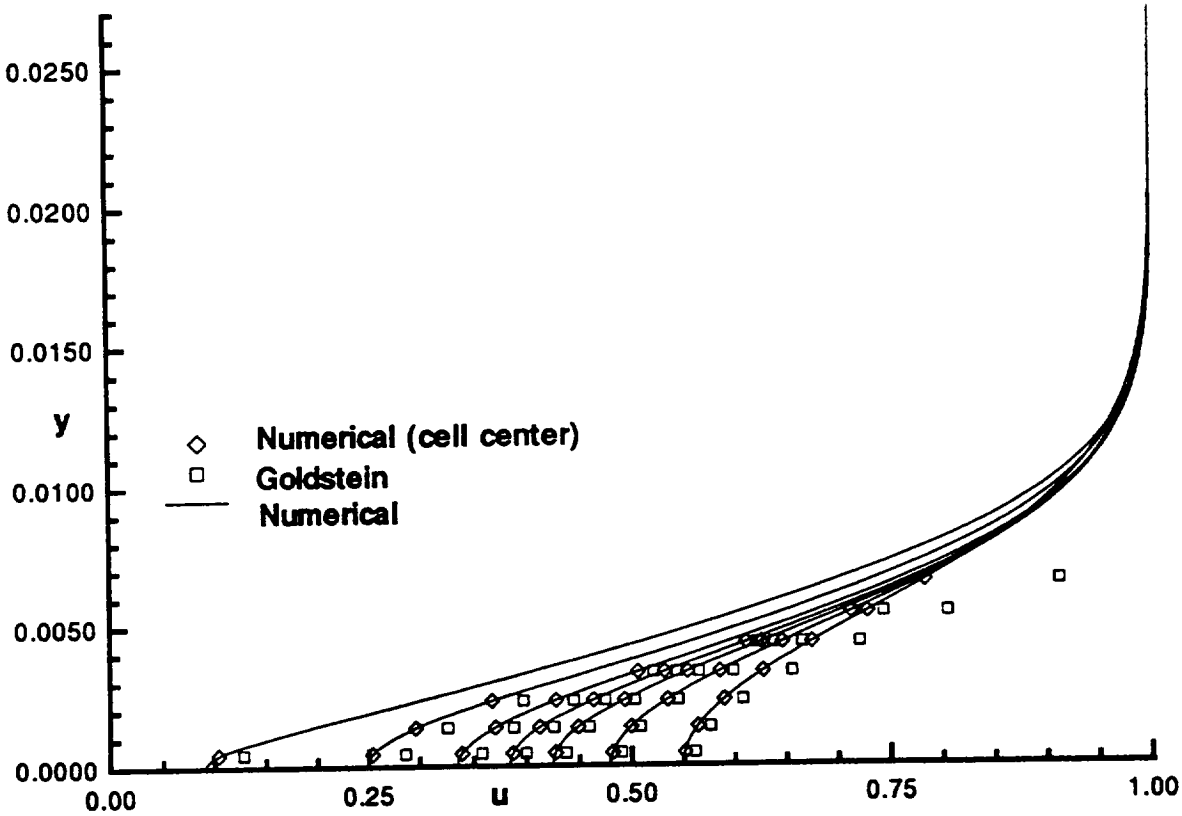

Figure 15b Comparison of predicted u velocity with Goldstein wake solution at x = 1.00333, 1.05, 1.10333, 1.15, 1.20333, 1.30333, and 1.49667. 240 x 40 Stretched Grid. Re = 100,000.

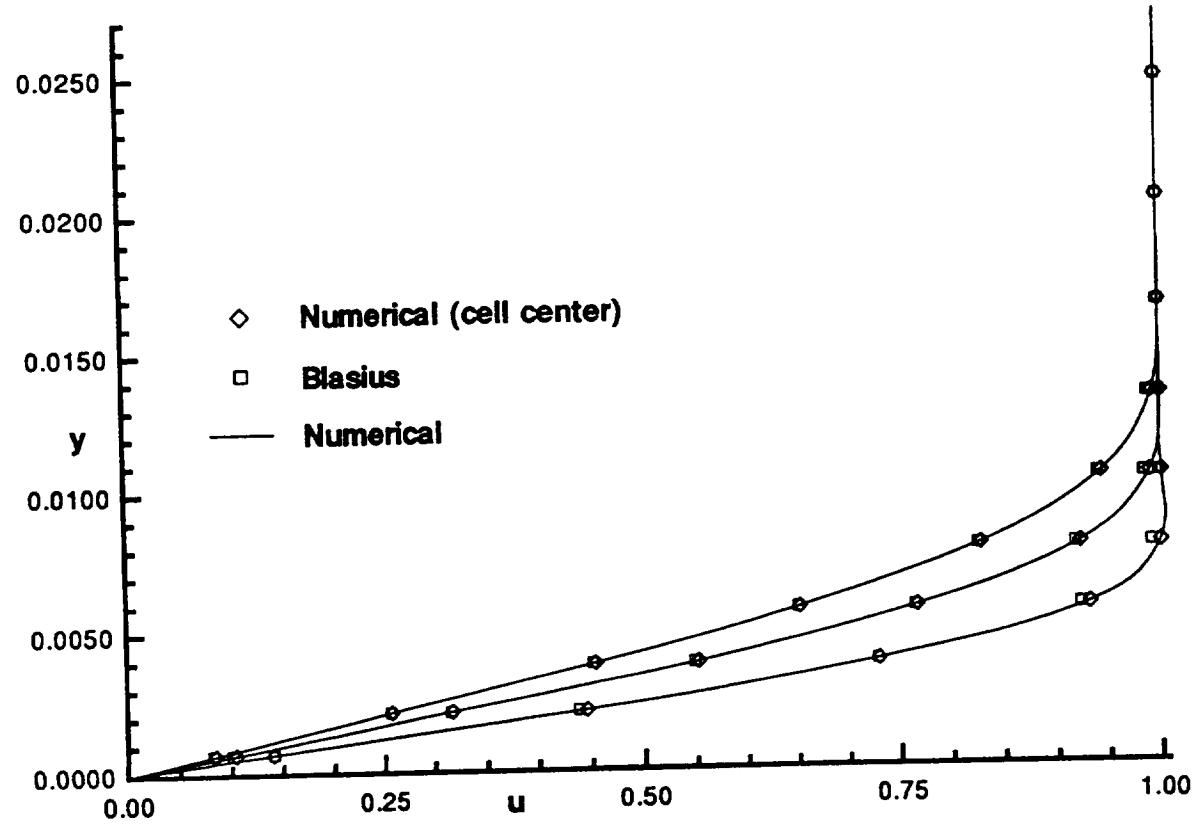

Figure 16a Comparison of predicted u velocity with Blasius solution at x = .25, .5, .75. 112 x 20 Stretched Grid. Re = 100,000.

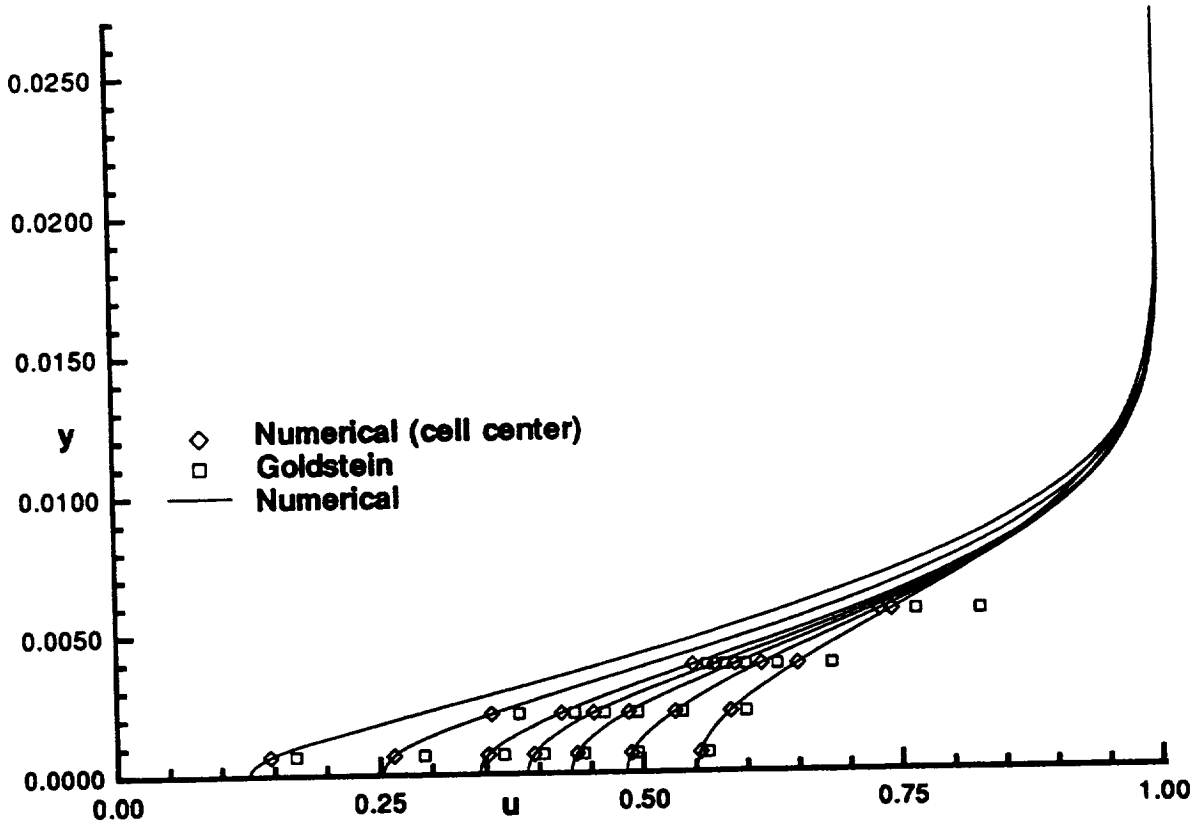

Figure 16b Comparison of predicted u velocity with Goldstein wake solution at x = 1.00714, 1.05, 1.10714, 1.15, 1.20714, 1.30714, and 1.49286. 112 x 20 Stretched Grid. Re = 100,000.

REPORT DOCUMENTATION PAGE

Form Approved
OMB No. 0704-0188

1. AGENCY USE ONLY (*Leave blank*)	2. REPORT DATE	3. REPORT TYPE AND DATES COVERED
	March 1996	Technical Memorandum

4. TITLE AND SUBTITLE

Further Development of a New, Flux-Conserving Newton Scheme for the Navier-Stokes Equations

5. FUNDING NUMBERS

WU-505-62-52

6. AUTHOR(S)

James R. Scott

7. PERFORMING ORGANIZATION NAME(S) AND ADDRESS(ES)

National Aeronautics and Space Administration
Lewis Research Center
Cleveland, Ohio 44135-3191

8. PERFORMING ORGANIZATION REPORT NUMBER

E-10162

9. SPONSORING/MONITORING AGENCY NAME(S) AND ADDRESS(ES)

National Aeronautics and Space Administration
Washington, D.C. 20546-0001

10. SPONSORING/MONITORING AGENCY REPORT NUMBER

NASA TM-107190

11. SUPPLEMENTARY NOTES

Responsible person, James R. Scott, organization code 2660, (216) 433-5863.

12a. DISTRIBUTION/AVAILABILITY STATEMENT

Unclassified - Unlimited
Subject Categories 02, 34, and 64

This publication is available from the NASA Center for AeroSpace Information, (301) 621-0390.

12b. DISTRIBUTION CODE

13. ABSTRACT (*Maximum 200 words*)

This paper is one of a series of papers describing the development of a new numerical approach for solving the steady Navier-Stokes equations. The key features in the current development are (i) the discrete representation of the dependent variables by way of high order polynomial expansions, (ii) the retention of all derivatives in the expansions as unknowns to be explicitly solved for, (iii) the automatic balancing of fluxes at cell interfaces, and (iv) the discrete simulation of both the integral and differential forms of the governing equations. The main purpose of this paper is, first, to provide a systematic and rigorous derivation of the conditions that are used to simulate the differential form of the Navier-Stokes equations, and second, to extend our previously-presented internal flow scheme to external flows and nonuniform grids. Numerical results are presented for high-Reynolds-number flow (Re = 100,000) around a finite flat plate, and detailed comparisons are made with the Blasius flat plate solution and Goldstein wake solution. It is shown that the error in the streamwise velocity decreases like $r^{\alpha}\,\Delta y^2$, where $\alpha \approx 0.25$ and $r = \Delta y/\Delta x$ is the grid aspect ratio.

14. SUBJECT TERMS

Flux; Flux-conserving; Navier-Stokes; Steady; Incompressible; Flat plate; Conservation element; Solution element

15. NUMBER OF PAGES

34

16. PRICE CODE

A03

17. SECURITY CLASSIFICATION OF REPORT	18. SECURITY CLASSIFICATION OF THIS PAGE	19. SECURITY CLASSIFICATION OF ABSTRACT	20. LIMITATION OF ABSTRACT
Unclassified	Unclassified	Unclassified	

National Aeronautics and
Space Administration

Lewis Research Center
21000 Brookpark Rd.
Cleveland, OH 44135-3191